

4-4-2003

On-screen pre-deblurring of digital images using the wavefront aberration function of the human eye to improve computer access for the visually impaired

Miguel Alonso

Florida International University

DOI: 10.25148/etd.FI13101605

Follow this and additional works at: <https://digitalcommons.fiu.edu/etd>

 Part of the [Computer Engineering Commons](#)

Recommended Citation

Alonso, Miguel, "On-screen pre-deblurring of digital images using the wavefront aberration function of the human eye to improve computer access for the visually impaired" (2003). *FIU Electronic Theses and Dissertations*. 1111.
<https://digitalcommons.fiu.edu/etd/1111>

This work is brought to you for free and open access by the University Graduate School at FIU Digital Commons. It has been accepted for inclusion in FIU Electronic Theses and Dissertations by an authorized administrator of FIU Digital Commons. For more information, please contact dcc@fiu.edu.

FLORIDA INTERNATIONAL UNIVERSITY

Miami, Florida

ON-SCREEN PRE-DEBLURRING OF DIGITAL IMAGES
USING THE WAVEFRONT ABERRATION FUNCTION OF THE HUMAN EYE
TO IMPROVE COMPUTER ACCESS FOR THE VISUALLY IMPAIRED

A thesis submitted in partial fulfillment of the

requirements for the degree of

MASTER OF SCIENCE

in

COMPUTER ENGINEERING

by

Miguel Alonso Jr.

2003

To: Dean Vish Prasad
College of Engineering

This thesis, written by Miguel Alonso Jr., and entitled On-Screen Pre-Deblurring of Digital Images Using the Wavefront Aberration Function of the Human Eye to Improve Computer Access for the Visually Impaired, having been approved in respect to style and intellectual content, is referred to you for judgment.

We have read this thesis and recommend that it be approved.

Malek Adjouadi

Frank Candocia

Armando Barreto, Major Professor

Date of Defense: April 4, 2003

The thesis of Miguel Alonso Jr. is approved.

Dean Vish Prasad
College of Engineering

Dean Douglas Wartzok
University Graduate School

Florida International University, 2003

DEDICATION

I dedicate this thesis to my family. Without the support of my Mother, Father, Sister, Grandmother, and my Girlfriend, this work would not have been possible.

ACKNOWLEDGMENTS

This thesis was supported by NSF grant EIA-9906600. I would like to acknowledge my thesis committee members, Dr. Armando Barreto, Dr. Malek Adjouadi, and Dr. Frank Candocia. They provided much insight and ideas which contributed to the development of my thesis. Without their help, I would not have been able to complete my Master's degree.

ABSTRACT OF THE THESIS

ON-SCREEN PRE-DEBLURRING OF DIGITAL IMAGES

USING THE WAVEFRONT ABERRATION FUNCTION OF THE HUMAN EYE TO

IMPROVE COMPUTER ACCESS FOR THE VISUALLY IMPAIRED

by

Miguel Alonso Jr.

Florida International University, 2003

Miami, Florida

Professor Armando Barreto, Major Professor

Traditional Optics has provided ways to compensate some common visual limitations (up to second order visual impairments) through spectacles or contact lenses. Recent developments in wavefront science make it possible to obtain an accurate model of the Point Spread Function (PSF) of the human eye. Through what is known as the “Wavefront Aberration Function” of the human eye, exact knowledge of the optical aberration of the human eye is possible, allowing a mathematical model of the PSF to be obtained. This model could be used to pre-compensate (inverse-filter) the images displayed on computer screens in order to counter the distortion in the user’s eye.

This project takes advantage of the fact that the wavefront aberration function, commonly expressed as a Zernike polynomial, can be generated from the ophthalmic prescription used to fit spectacles to a person. This allows the pre-compensation, or on-screen deblurring, to be done for various visual impairments, up to second order (commonly known as myopia, hyperopia, or astigmatism). The technique proposed towards that goal and results obtained using a lens, for which the PSF is known, that is

introduced into the visual path of subjects without visual impairment will be presented. In addition to substituting the effect of spectacles or contact lenses in correcting the low-order visual limitations of the viewer, the significance of this approach is that it has the potential to address higher-order abnormalities in the eye, currently not correctable by simple means.

TABLE OF CONTENTS

CHAPTER	PAGE
1 Introduction.....	1
1.1 Problem Overview	1
1.2 Problem Statement.....	3
1.3 Image Data	4
1.4 Pre-compensation.....	6
1.5 Testing Methods.....	7
1.6 Thesis Overview	8
2 Human Vision	9
2.1 Anatomical Description of the Human Eye.....	9
2.2 Optical System of the Human Eye.....	12
2.3 Image Formation for Optical Systems	15
2.3.1 Classical Optics.....	16
2.3.2 Wave Theory of Image Formation.....	19
2.3.3 Fourier Optics	23
2.4 Human Eye as an Imaging System	25
2.5 Wavefront Aberrations and Zernike Polynomials	28
2.6 Second Order Aberrations.....	30
2.6.1 Emmetropia.....	31
2.6.2 Hyperopia.....	32
2.6.3 Myopia	33
2.6.4 Astigmatism	34
2.7 High Order Aberrations	36
2.8 Obtaining the Analytical PSF	37
3 Clinical Visual Optics	39
3.1 Visual Acuity	39
3.2 Eye Chart Descriptions	41
3.3 Evaluation of Visual Performance	44
4 Deconvolution.....	49
4.1 Van Cittert's Method	50
4.2 Non-Negative Least Squares.....	51
4.3 Minimum Mean Square Error Filtering	52
5 Experiment Description	55
5.1 Overview	55
5.2 System Elements.....	57
5.2.1 Monitor	57
5.2.2 Camera	58
5.2.3 Lens.....	60

5.2.4	Personal Computer.....	61
5.3	Introduction of Wavefront Aberration.....	61
5.3.1	Scaling.....	62
5.3.2	Determining the true Wavefront Aberration.....	63
5.4	Eye Chart Implications	71
5.4.1	Resolution of the Minimum Angle	71
5.5	Testing Procedure	72
6	Results and Discussion	77
6.1	Simulated Experiment for -6.00 Diopter Sphere Lens.....	77
6.2	Results.....	81
6.2.1	Standard Test	81
6.2.2	Blurred Test	82
6.2.3	Pre-compensated Test	84
6.3	Discussion of Results.....	85
7	Conclusion	89
	List of References	91
	Appendices.....	94

LIST OF TABLES

TABLE	PAGE
Table 3-1: The log of the Minimum Angle Resolved (logMAR) scale, corresponding minimum angles of resolution, and equivalent decimal V and Snellen distance acuities.....	44
Table 5-1: Gateway VX1120 Digital Monitor Specifications [8]	58
Table 5-2: SONY Mavica Specifications	59
Table 6-1: Results of the Standard Test for 28 eyes	81
Table 6-2: Mean and Standard Deviation for Standard Test	82
Table 6-3: Results of the Blurred Test for 28 eyes	83
Table 6-4: Mean and Standard Deviation for Blurred Test	84
Table 6-5: Results of the Pre-compensated Test for 28 eyes.....	84
Table 6-6: Mean and Standard Deviation for Pre-compensated Test.....	85

LIST OF FIGURES

FIGURE	PAGE
Figure 1-1: 64X64 Two-Dimensional representation of letter A.....	5
Figure 1-2: Beige letter “A” (a) Red grayscale (b) Blue grayscale (c) Green grayscale	5
Figure 1-3: Retinal Image resulting from convolution of Object with the PSF	6
Figure 1-4: Pre-compensation Process.....	6
Figure 1-5: ETDRS Chart "R"	7
Figure 2-1: A cross-sectional, anatomically correct drawing of the human eye. (Reproduced from [28])	10
Figure 2-2: Formation of the retinal image depicted as change in the curvature of incident wavefronts or as bending of light rays, assuming the eye's optical system were perfect (a) or imperfect (b) (Reproduced from [28])	15
Figure 2-3: Geometrical optics rules for the change in wavefront vergence due to propagation in a homogeneous medium (a) or refraction by an interface between two media of different refractive indices (b) (Reproduced from [28]).....	16
Figure 2-4: Snell's law for refraction yields the formula for image magnification (Reproduced from [28])	18
Figure 2-5: Example of an expanding (a) and collapsing (b) wavefront through an aperture (Reproduced from [28])	20
Figure 2-6: Huygens's theory of wavefront propagation (Reproduced from [28]).....	21
Figure 2-7: Geometry for computing the contribution of Huygen's wavelet at point S to the amplitude of light at point R (Reproduced from [28])	22
Figure 2-8: Black Box of the imaging process in the human eye (Modified from [12]).....	26
Figure 2-9: Wavefront aberration deviation from the pupil sphere; defined as either distance ab or $a'b$, depending on precise definition. For the range of the typical wavefront, these distances are essentially equal (reproduced from [25]).....	29

Figure 2-10: Parallel light rays focus on the retina in an emmetropic, behind the retina in an hyperopic eye, and in front of the retina for a myopic eye	30
Figure 2-11: Demonstration of astigmatism. Light rays focus at one focal distance in one plane (AC) , and at another focal distance in the plane at a right angle (BD).	31
Figure 2-12: Example of the wavefront aberration for an Emmetropic Eye. Values are normalized over the pupil area. Notice that there is no deviation from 0 implying that the exiting wavefront did not suffer any type of distortion.	32
Figure 2-13: Example of the wavefront aberration for a hyperopic eye.....	33
Figure 2-14: Example of the wavefront aberration for a myopic eye.....	34
Figure 2-15: Example of the wavefront aberration for a 45/135 astigmatic eye.	35
Figure 2-16: Example of the wavefront aberration for a 180/90 astigmatic eye.	36
Figure 2-17: Example of the wavefront aberration for a real eye, suffering from advanced keratoconus.	37
Figure 3-1: The Snellen visual acuity test chart.....	40
Figure 3-2: An example of a Bailey-Lovie logMAR eye test chart using 'sloan' letters.....	43
Figure 3-3: Relationship between AMA visual efficiency, and Snellen visual distance acuity in decimal.....	47
Figure 5-1: Gateway VX1120 22-inch Monitor showing the third line of ETDRS Eye Test Chart.....	57
Figure 5-2: Sony Mavica MVC-FD95 Digital Still Camera.....	59
Figure 5-3: Optical grade lens with Sphere = -6.0.....	60
Figure 5-4: Wavefront aberration for the -6.0 D lens used.....	61
Figure 5-5: Image of approximated point source.....	64
Figure 5-6: Resulting, blurred image of point source due to the introduction of the -6.0 lens.....	65

Figure 5-7: Resulting PSF from deconvolving figure 5-4 from 5-5 (Enhanced for Display)	65
Figure 5-8: Two-dimensional representation of figure 5-4.....	66
Figure 5-9: Two-dimensional representation of figure 5-5.....	66
Figure 5-10: Two-dimensional representation of figure 5-6.....	67
Figure 5-11: One-dimensional slice through the center of the Input Image.....	67
Figure 5-12: One-dimensional slice through the center of the Output Image.	68
Figure 5-13: One-dimensional slice through the center of the PSF Image.....	68
Figure 5-14: Analytical PSF of -6.0 lens found through fitting of empirical PSF	69
Figure 5-15: Two-dimensional mesh of figure 5-13.....	70
Figure 5-16: One-dimensional slice of Analytical PSF	70
Figure 5-17: Experimental Setup (a) Top - Standard Eye Test, No Aberration Present (b) Middle – Blurred Eye Test, Aberration Present (c) Bottom – Pre-compensated Eye Test, Aberration Present, Correct Wavefront.....	73
Figure 5-18: Image of Subject participating in the Study - After the introduction of the Lens.....	75
Figure 5-19: Image of Subject - Before the Introduction of the Lens	75
Figure 5-20: Image of Subject - Also, Before the Introduction of the Lens.....	76
Figure 6-1: Analytical PSF generated for testing	77
Figure 6-2: Digital Image of Eye Test Chart Line 1	78
Figure 6-3: Simulation of Digital Image of Eye Test Chart Line 1 viewed through the -6.0 D lens.....	78
Figure 6-4: Pre-compensated Eye Test Chart Line 1	79
Figure 6-5: Simulated Retinal Image, that is, what the viewer will see when looking at Figure 6-3 through the -6.0 D lens.....	79

Figure 6-6: Mesh of Figure 6-4 without post processing.....	80
Figure 6-7: Figure 6-4 after post processing.....	80
Figure 6-8: Visual Acuity vs. Eye ID	86
Figure 6-9: Relative Improvement of Visual Efficiency for the subjects.....	87
Figure 6-10: Histogram of Improvement of Visual Efficiency	88

1 INTRODUCTION

Over the past few centuries, developments in research and advancements in technology have led to the use of artificial means to overcome visual limitations in human beings. These visual limitations, however minute, hinder the ability to perform day to day activities, such as reading and writing. Optical lenses have been used to overcome visual limitations, such as myopia or hyperopia, in one way or another since the XIII Century. Furthermore, the ability to characterize such limitations, such as astigmatism, and the means to compensate for them has existed since the XIX Century. Although many advances in vision correction have existed for centuries, it was not until recently, ([27]), that the proposal to characterize and correct complex imperfections of the human eye was presented. The current, state-of-the-art technology emerging in ophthalmology has enabled doctors to correct such impairments through physical means, such as contact lenses or glasses, as well as through surgery, such as LASIK (Laser-Assisted In-Situ Keratomileusis). There are instances, however, when these solutions cannot completely correct visual impairments. It is for these individuals that this thesis work is targeted. The procedure being investigated would allow some low vision users, for whom present day technology cannot help, overcome their impairments when accessing computers with a digital display or monitor.

1.1 Problem Overview

Vision is the primary source of information about the surrounding environment that humans have. Through the evolutionary process, humans have developed a very refined sense of visual perception, seeing in three dimensions with high resolution and color [24].

The sense of sight is so important that, when limited by age or disease, it limits a person's ability to perform otherwise ordinary tasks, such as interacting with a computer system.

Visual perception of objects in the physical world is determined by the formation of their images on the retina, located inside the human eye [28]. However, the natural visual system of some individuals does not accurately map images from the outside world onto their retinas. The most common of these visual impairments include myopia, hyperopia, and astigmatism. All of them result in a retinal representation of a point of light that is not confined to a single point on the retina. The distortion in the mapping of external images onto the retina is termed "wavefront aberration function." Myopia, hyperopia, and astigmatism are referred to as low-order aberrations because the distortion they introduce can be modeled by first or second order Zernike polynomials. Currently, spectacles or contact lenses correct these low-order impairments by modifying external images before they reach the eye.

There are cases, however, in which the low-order Zernike model is not sufficient to describe the aberration of the eye. With the recent advances in Wavefront Sensing technology and the emergence and availability of so-called "Wavefront Analyzers", it is now feasible to accurately model the high-order aberrations present in each person's eye and thus obtain good models of various aberrations currently not correctable through conventional means (e.g., spectacles, contact lenses). Using these models, it would be possible to provide persons with currently uncorrectable aberrations, a new alternative to enhance their interaction with computers.

In contrast with the optical correction of visual limitations, the approach described here is based on modifying the image at its source, i.e., in applying image processing

modifications on the image to be displayed on-screen before it is shown to the user, using the knowledge of his/her wavefront aberration function. The aim of the pre-compensation proposed is to modify the intended display image in a way that is opposite to the effect of the wavefront aberration of the eye. Once this is achieved, the result is displayed to the viewer so that the effect of the wavefront aberration in the viewer's eye will "cancel" the pre-compensation, resulting in the projection of an undistorted version of the intended image on the retina.

1.2 Problem Statement

Out of the five senses that humans have, vision is the one sense that human beings use the most in order to perform successfully in any environment. Consequently, if a person has limited visual capabilities, resulting from disease, age, or genetics, it would be beneficial if there were a method for enhancing his/her interaction with computers. This is particularly true in today's world where the personal computer (PC) has become an integrated part of the daily efficient function of people. To this end, this thesis proposes that visual aberrations, described by their Zernike polynomials, can be compensated by displaying digital images modified using knowledge of the wavefront aberrations on a PC monitor or digital display. The method in which the proposed digital images are generated is through deconvolution of the intended images, that is, the images which the person is supposed to see. In previous research, the proposed method of deconvolving images has not been applied to compensation of aberrations, but rather to reconstruction of images that are degraded by known or unknown means. Thus, this work is an effort to

develop a new, innovative approach to vision correction geared for enhancing human-computer interface.

Several methods of deconvolution will be explored as the primary mechanism for generating the pre-compensated images to be displayed to the user. This method will be evaluated with human subjects using a standard optometrist's eye test, before and after compensations of visual aberration.

1.3 Image Data

The images used will be represented as two-dimensional matrices, with values in the matrix ranging from 0 to 255. Figure 1-1 shows the two-dimensional mesh of a 64 by 64 pixel image of a white letter "A" on a dark background. For the purposes of this research, the images will be grayscale images, thus the value of 255 represents the color white, and the value of 0 represents the color black. All other values between 0 and 255, non-inclusive, correspond to 254 gray levels.

Grayscale images were chosen over color or Red-Green-Blue (RGB) images because of the way that grayscale images are represented in the PC. Grayscale images, as mentioned above, may be defined as a two-dimensional function, $f(x, y)$, where x and y are the spatial coordinates, and the value of f at any pair of coordinates (x, y) is called the intensity or gray level of the image at that point [11].

Color images on the other hand, consist of three intensity matrices, with each matrix representing one of the three colors, Red, Green, or Blue. Evidently, the processing of color images is three times as computationally intensive as the processing of grayscale images.

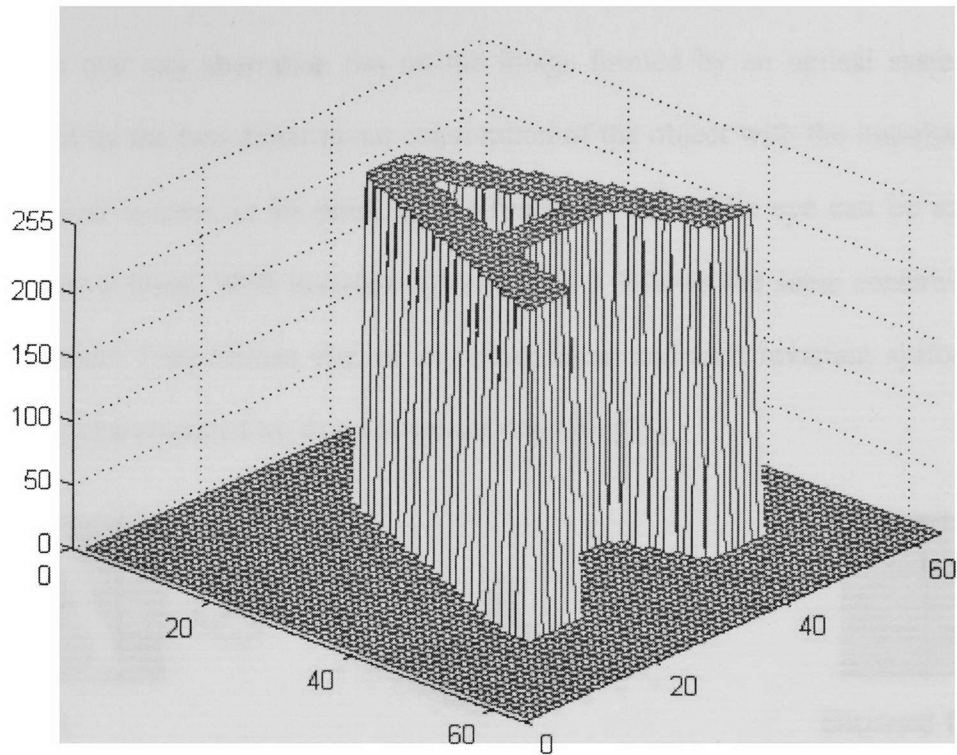


Figure 1-1: 64X64 Two-Dimensional representation of letter A

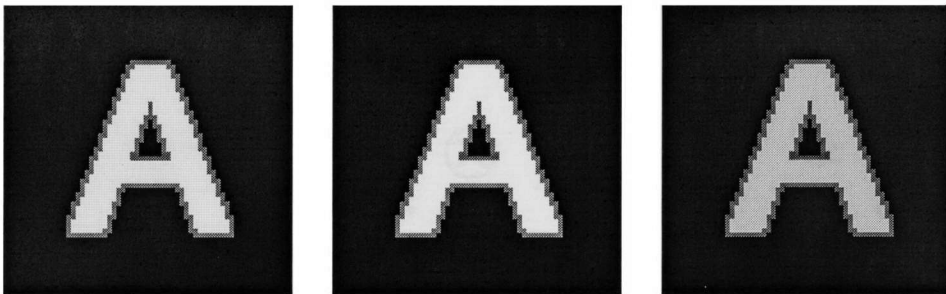


Figure 1-2: Beige letter “A” (a) Red grayscale (b) Blue grayscale (c) Green grayscale

Figure 1-2 shows the three individual matrices of the same letter “A” in color, that is, there are three matrices representing the picture, not one. The color image of “A” is a beige letter A on a black background.

1.4 Pre-compensation

The effect that any aberration has on the image formed by an optical system can be represented by the two-dimensional convolution of the object with the impulse response of the optical system, or its point spread function (PSF). The eye can be assumed to approximate a linear, shift invariant system, thus it follows the same constraints of any optical system. The human eye, as any other linear and shift invariant system, can be completely characterized by its point spread function [15].

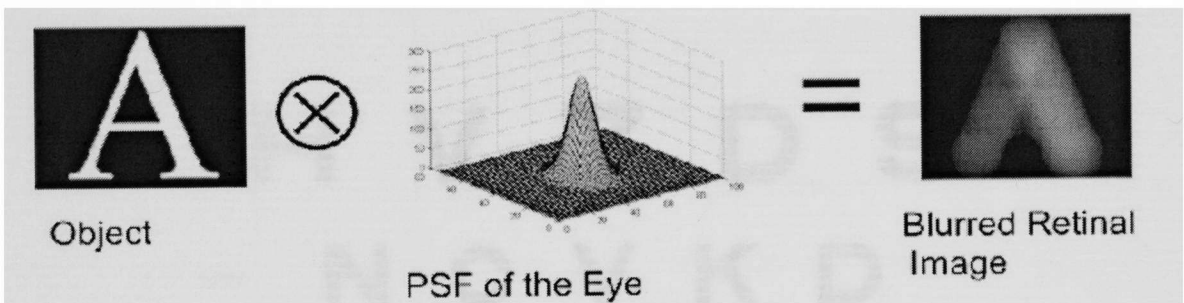


Figure 1-3: Retinal Image resulting from convolution of Object with the PSF

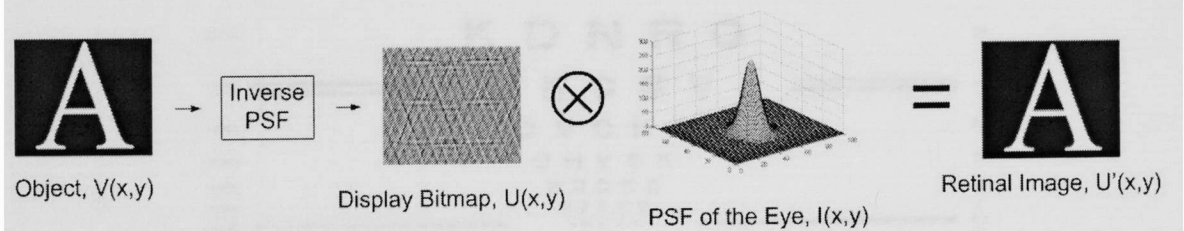


Figure 1-4: Pre-compensation Process

According to this model, the image formed on the retina results from the convolution of the scene or in this case the digital image which is intended to be projected onto the retina, with the point spread function of the eye (see figure 1-3). The

point spread function of the eye can be found through the Wavefront Aberration function of the eye.

If the PSF of a subject's eye is known a-priori, it would be possible to pre-compensate the image shown to the user, through deconvolution of the intended digital image from the PSF. This would counter the effect of the PSF on the intended image and allow the image projected on the retina to be distortion-free. This concept is illustrated in figure 1-4.

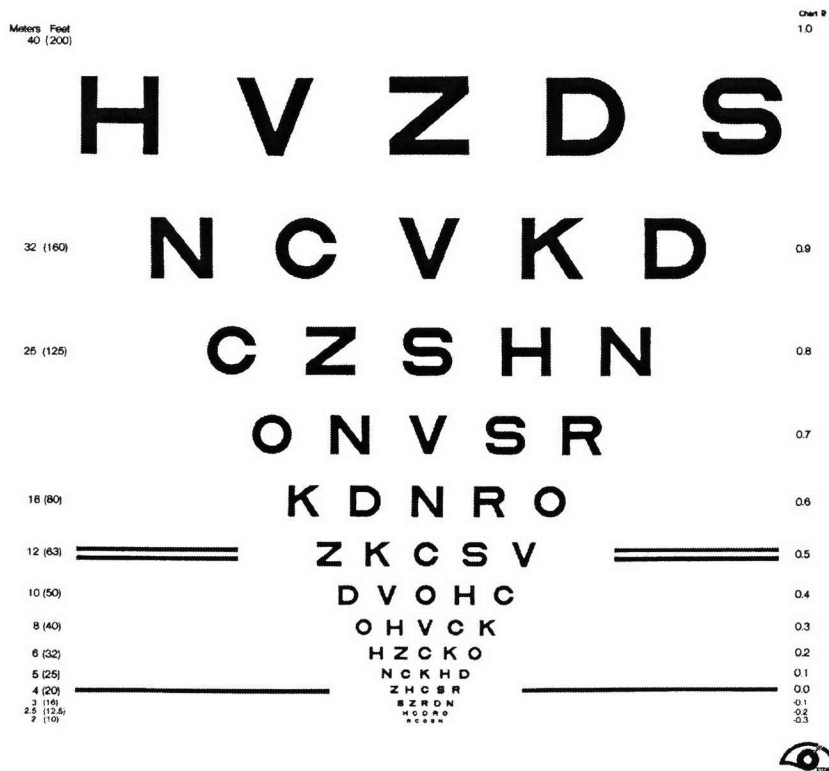


Figure 1-5: ETDRS Chart "R"

1.5 Testing Methods

The proposed method of overcoming the aberrations introduced by the human eye will be evaluated using a digitally reproduced visual acuity chart, known as an ETDRS (Early

Treatment of Diabetic Retinopathy Study) chart. In particular, this chart is referred to as chart “R” (see figure 1-5).

This is the preferred eye chart used in diagnosing visual acuity because the letters are uniformly spaced on each line and the size of the letter decreasing from line to line uniformly at a ratio of 1.25:1, or approximately 80% [3].

1.6 Thesis Overview

This thesis is structured in the following manner. Chapter 2 is concerned with describing the Human Visual system. It covers an outline of the physiology of the eye, and the corresponding foundations of image formation in the eye, as well as a description of the wavefront aberration function and its mathematical representations. Chapter 3 details the clinical aspects of vision, including visual acuity, eye charts, and methods of evaluation of visual performance. Chapter 4 presents the proposed deconvolution techniques investigated, presenting the Van Cittert’s, Non-negative Least Squares, and Minimum Mean Squared approaches. In addition, the reasons behind choosing the latter as the primary method for achieving the proposed pre-compensation will be explained. Chapter 5 describes the method followed for the evaluation of the project, from the elements of the experiments to the testing procedure used to evaluate the proposed methods of pre-compensation. Chapter 6 presents the data, simulated and empirical, resulting from implementation and testing of the pre-compensation with 14 subjects, corresponding to 28 eyes. This chapter also includes a discussion of the experimental data recorded. Finally, Chapter 7 summarizes the conclusions and offers some potential applications for this work.

2 HUMAN VISION

Human vision begins with the formation of an optical image of objects in the external world upon the retina, a mosaic of light sensitive photoreceptors [28]. Because the first step in human vision is the formation of images onto the retina, any type of imperfections in the optical system of the eye which create these projections have the potential to affect every part of the visual process.

The second step in visual processing is the sampling of this optical information by the retina, a “sensitive screen on which the optical image should fall when in sharp focus” [3]. The retina is composed of rods, photoreceptors sensitive to color, and the rods, which are mainly responsible for vision in the dark.

This thesis concerns itself with only the optical portion of the eye’s aberrations. That is, only the physics of image formation will be considered relevant in formulating the general analysis and understanding of the convolutional and deconvolutional processing. Potential aberrations introduced by the retina after the image has formed on it will not be addressed. The method of pre-compensation described in this thesis attempts to account only for the imperfections in the optical system of the eye.

2.1 Anatomical Description of the Human Eye

The human eye is composed of many elements, all contributing in some form or another to the overall process of human vision. An anatomically correct cross-sectional view of the human eye is shown in figure 2.1. The basic elements of the eye are the cornea, the anterior chamber, iris, pupil, crystalline lens, and the retina.

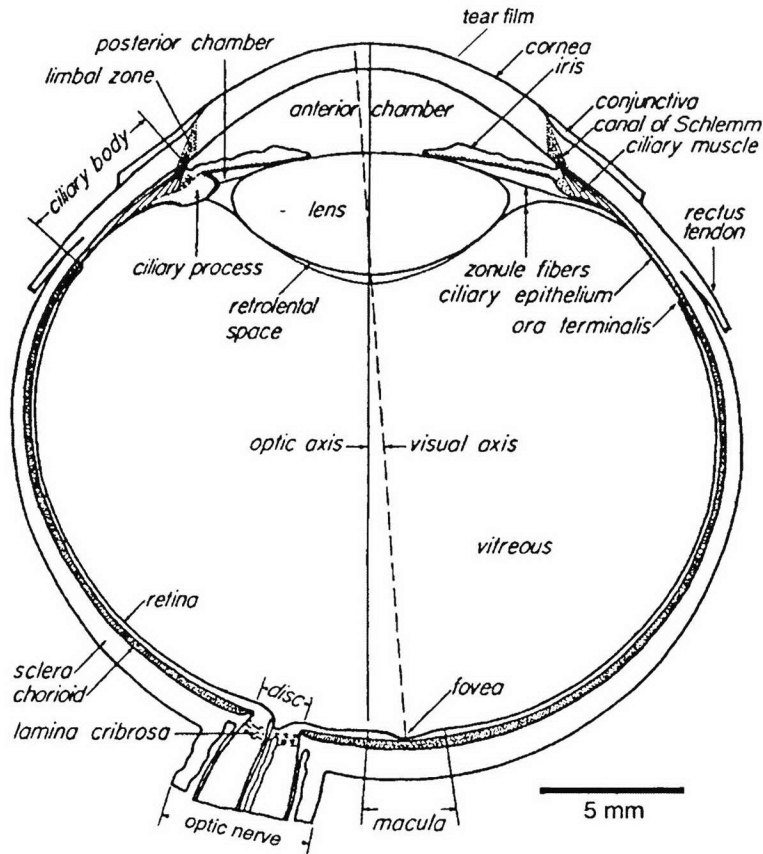


Figure 2-1: A cross-sectional, anatomically correct drawing of the human eye. (Reproduced from [28])

The cornea is a highly transparent structure approximately 12 mm in diameter and slightly smaller vertically than horizontally. The center thickness is about 0.5 mm [3]. A thin layer of lacrimal fluid normally covers the anterior surface of the cornea, but it is too thin to substantially affect the refractive power of the cornea as whole. The cornea accounts for over two thirds of the total power of the eye [3].

The anterior chamber of the human eye is the cavity that lies behind the cornea and in front of the crystalline lens. It is filled with a liquid called the aqueous humour which is composed primarily (98%) of water [3]. The depth of this chamber is measured

along the eye's optical axis, and is strictly "the distance from the posterior vertex of the cornea to the anterior surface of the crystalline lens" [3]. The depth of this chamber is important because it affects the total power of the eye's optical system.

The iris and the pupil control the amount of light that enters the eye. The pupil, an approximately circular opening in the iris, reacts under normal conditions to [3]:

1. A change in luminance. This is termed the 'direct' reflex.
2. A change in luminance applied to one eye only, producing a 'consensual' reflex in the opposite eye.
3. Near fixation accompanied by papillary contraction.

The size of the pupil decrease uniformly as age increases. The rate at which it decreases does slowdown, however, later in life. For the eye in total darkness, 7.6 mm at age 10, 6.2 mm at age 45, and 5.2 mm at age 80, can be taken to be typical pupil diameters varying with age. In lit situations, the pupil reduces in size to 4.8 mm at age 10, 4.0 mm at age 45, and 3.4 mm at age 80 [3].

The crystalline lens, located behind the iris is responsible for providing the balance of the eye's refractive power. Additionally, it provides a mechanism for focusing at various distances [3]. During childhood and early adulthood, the internal lens of the eye is so flexible that its anterior surface can bulge forward, increasing its optical power allowing it to focus on objects that are closer. This change in shape occurs as tension on the supporting zonule fibers is released in response to forward movement of the ciliary processes caused by contraction of the ciliary muscle [9],[16]. This ability of the eye to increase its focal power is called accommodation.

The lens has an approximate diameter of 9 mm and is biconvex, the radius of its anterior surface being about 1.7 times that of its posterior surface [3]. When the lens is in an unaccommodated state, the center thickness has traditionally been taken to be about 3.6 mm for a young adult. As accommodation changes the lens, both surfaces assume more steeply curved form [3], thus changing its refractive power.

The retina, the final major component in human vision, is a photosensitive curved surface which lies about 17 mm behind the lens. The retina's ability to distinguish detail is not uniform over the entire extent to which it reaches. It is at its maximum in the macular region. This macular region is an approximately circular area with a diameter of about 1.5 mm containing a smaller central region called the fovea, populated entirely by cones. "It is at the fovea that the eye attains its maximum resolving power. When an object engages visual attention, the two eyes are instinctively turned so that the image lies on each fovea" [3]. Thus, this thesis concerns itself with images directly on visual axis, as well as optical axis. The images used will subtend less than 5 minutes of arc of visual angle, thus projecting the image directly on or near the foveal region. This stipulation also ensures that the aberrations caused by peripheral vision will not confound the main optical aberrations, which are the aim of the pre-compensation process proposed by this thesis.

2.2 Optical System of the Human Eye

In its resting state, that is, when the eye is fixed on a distant point, two-thirds of the optical power of the eye is provided by refraction of light by the cornea, and the remaining third is provided by the internal structures of the eye, such as the lens [28]. The

internal lens however, as mentioned earlier, is capable of bending and changing its shape to provide additional focusing power when the eye is fixed on close objects [28].

The cornea, the first surface to interact with the light rays, alone provides about +43 Diopters (D) of refractive power, over two-thirds of the total power of the eye [3]. The principle reason for this is that the index of refraction of the cornea is very different from that of air [13].

On the other hand, the total refractive power of the eye's lens, as it normally lies in the eye surrounded by fluid on both sides, is only +20 D, about one-third of the total refractive power of the eye's optical system [13]. If the eye's lens were to be removed and then surrounded by air, the refractive power of the lens would increase by about six times. The main reason for this is that the index of refraction for the fluid surrounding the lens is not much different from the lens itself [13].

If all of the refractive surfaces of the eye, from the cornea, to the crystalline lens, were algebraically added together and considered to be one lens, the total refractive power of the eye, when accommodated for distant vision, would be about +59D [13].

If an eye produces a clearly focused image on the retina for distant objects when the lens has minimum power, it is said to be emmetropic. At birth, the human eye is small. It grows rapidly over the first three years of life, and by about three years of age, the eye is nearly adult sized [3]. During this period of early childhood, a growth process called emmetropization aims to keep the eye clearly focused for distant targets when the eye is its resting state [14], [31].

The accommodative range for the eye is more than 10D in a young eye, but this value declines at a constant rate throughout adulthood and eventually disappears (a

condition called presbyopia) at about fifty five years of age when the lens has become completely inflexible [9]. The power of accommodation decreases from about 14 D in a child to less than 2 D by the time the person is fifty five, and it decreases to about 0 D at age 70 [13].

Once a person has reached the state of presbyopia, the eye remains permanently focused at a fixed distance depending on the physical characteristics of each person's eye [13]. The eye can no longer accommodate for both near and far vision, making the use of bifocal glasses necessary. The bifocals, with the upper segment normally focused for far-seeing and the lower segment for near-seeing, provide some correction.

In addition to changes that occur in all eyes due to age, there are other changes that occur in a significant minority of eyes. Many eyes grow excessively in the axial direction during childhood, causing the retinal image of distant objects to be formed in front of the retina [13], [28]. The term for this type of aberration is near-sighted, or myopic, "a condition which easily corrected weakening the optical power of the eye by wearing a spectacle or contact lens with negative power" [28]. The opposite condition, or far-sightedness, is called hyperopia. In this case, the image formed by the eye is behind the retina. This eye often can accommodate, even in the presence of hyperopia. Other eyes may have a cornea or lens that is not radially symmetric, causing contours of different orientations to produce different images at different distances. This condition is called astigmatism and can be corrected by spectacle lenses that have the same contours but opposite sign.

Although other defects do occur in the human population, the only optical defects or aberrations that are routinely corrected by spectacles or contact lenses are myopia,

hyperopia, presbyopia, and astigmatism. “This traditional practice is likely to change in the near future, however, as new technologies for measuring and correcting the eye’s aberrations mature” [21]. This thesis takes advantage of the fact that a more precise model of the eyes aberrations is becoming readily available.

2.3 Image Formation for Optical Systems

If the eye’s optical system were perfect, it would focus all of the rays of light from a distant point entering the eye into a single image point on the retina (See figure 2.2). In order to find where the point is located, we can apply the laws of paraxial optical theory to describe the idealized case of perfect imaging. But in the real world, the eye is not a perfect optical instrument. It suffers from three types of optical imperfections which are not treated by paraxial theory: aberrations, diffraction, and scattering [28]. Even though the mechanisms of the imperfection are different in each case, the overall effect of these imperfections is to spread light across the retina, as shown in figure 2.2(b). Additionally, the spatial distribution of light intensity in the image can be understood with the concepts and computational tools of Fourier analysis [12].

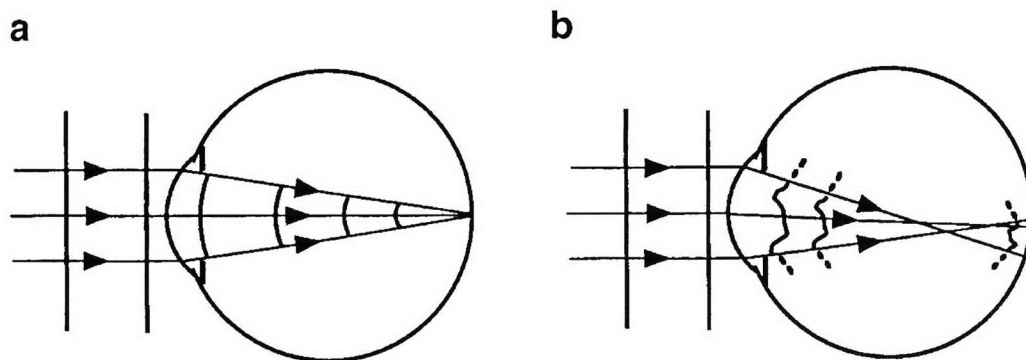


Figure 2-2: Formation of the retinal image depicted as change in the curvature of incident wavefronts or as bending of light rights, assuming the eye's optical system were perfect (a) or imperfect (b) (Reproduced from [28])

2.3.1 Classical Optics

Light is an electromagnetic field that propagates energy through space as a traveling wave and at any point in space, the amplitude of this field modulates sinusoidally in time. The energy of this wave propagates outwards from its source in the form of traveling waves, much like the ripples encountered when a stone is cast into a perfectly calm pond. The direction of propagation of the advancing wavefront at any given point in space is specified by a ray emerging from the source that is perpendicular to the wavefront at the point [25].

In the paraxial domain, wavefronts of light are assumed to have a spherical shape that is characterized by a center of curvature and radius of curvature. The image formed by a collapsing spherical wavefront is a single point at the center of curvature with the determination of image location being the same problem as finding the center of curvature of a refracted wavefront [28].

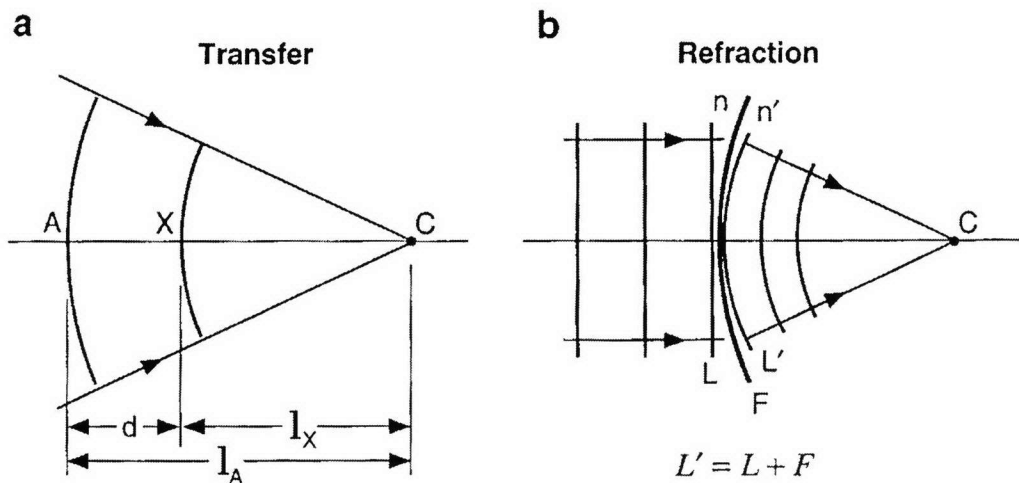


Figure 2-3: Geometrical optics rules for the change in wavefront vergence due to propagation in a homogeneous medium (a) or refraction by an interface between two media of different refractive indices (b) (Reproduced from [28])

This problem can be easily solved if the wavefront is described in terms of its curvature (i.e., the inverse of the radius of curvature). Therefore, the vergence L of a spherical wavefront is defined as:

$$L = n/r \quad (2.1)$$

where n is the index of refraction of the medium in which the wavefront exists, and r is the radius of curvature of the wavefront [28].

There are two rules governing the imaging process: the transfer rule and the refraction rule. In order to derive the transfer rule as shown in figure 2.3, the linear relationship

$$l_X = l_A - d \quad (2.2)$$

is stated in terms of vergence by substituting $L_A = n/l_A$ and $L_X = n/l_X$ to get

$$L_X = \frac{L_A}{1 - (d/n)L_A}. \quad (2.3)$$

In the context of described in Figure 2-3, l_A should never be equal to d . If they were to be equal, L_X would diverge towards infinity. But, if they were to be equal, this equation would no longer be applicable because the wavefront would have traveled to the end of its path, converging at point C.

The refraction rule describes how a wavefront changes upon entering a new medium. The interface between the two different media can be any shape, but for analysis in the paraxial domain, the shape is approximated by a spherical surface with radius of curvature r [28]. The surface power is proportional to the reciprocal of the focal length. Thus, the refractive power F of a surface is

$$F = \frac{n' - n}{r} \quad (2.4)$$

where n is the refractive index of the medium [3]. The unit of focal power is the diopter (D), expressed as the inverse of the focal length of the surface in meters.

If a wavefront with vergence L incidents on a surface with a power of F , then immediately after entering the new medium, the wavefront has a vergence L' given by

$$L' = L + F \quad (2.5)$$

The focal length of a convex lens is defined as the distance beyond the lens at which parallel rays or similarly wavefronts converge to a common focal point. The relationship of focal length of the lens, the distance of a point source of light, and the distance of focus is expressed by the following:

$$\frac{1}{f} = \frac{1}{a} + \frac{1}{b} \quad (2.6)$$

where f is the focal length, a is the distance of the point source of light from the lens, and b is distance of focus on the other side of the lens [13].

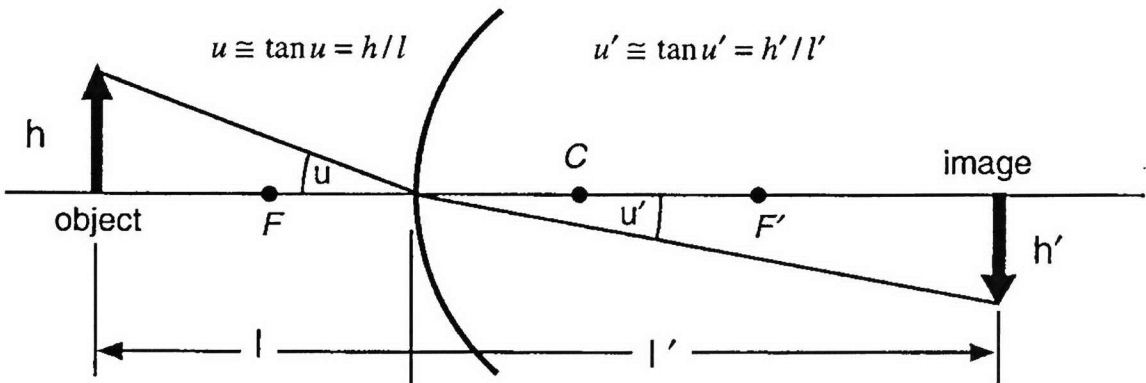


Figure 2-4: Snell's law for refraction yields the formula for image magnification (Reproduced from [28])

In order to determine the image of object points off axis but still within the paraxial domain, Snell's law of refraction can be used to derive the magnification (m) formula [28], [13].

$$m = \frac{I'}{I} \quad (2.7)$$

Outside the paraxial domain of perfect imaging, aberrations are said to exist when the refracted rays from an object point intersect the image plane at different locations, causing the light to be spread out over an area. This distribution of light intensity in the image of a point source, called the point spread function (PSF), is a fundamental characterization of the system. This PSF is analogous to the impulse response for a one-dimensional system. Knowledge of this PSF is of great value because it allows for the computation of the image of arbitrary object as the superposition of individual PSFs from every point in the object [28].

There are two major sources of aberrations in the human eye, both relating to the size of the pupil. When the size of the pupil diameter is about 2 mm or less, the major contribution to distortion of the retinal image is a phenomenon known as diffraction. When the pupil diameter is larger than 2 mm, the aberrations of the optical system hinder perfect image formation on the retina. The wave theory of image formation accounts for both of these issues.

2.3.2 Wave Theory of Image Formation

According to the wave theory of image formation, "the perfect image of a point object is formed by a collapsing hemispherical wavefront with center of curvature located in the image plane" [28]. An aberrated wavefront is thus characterized by its deviation from this

perfect wavefront. Thus, the wavefront error can be used to describe the aberrations introduced by an optical system producing a wavefront that departs from the ideal wavefront produced by a “perfect” optical system.

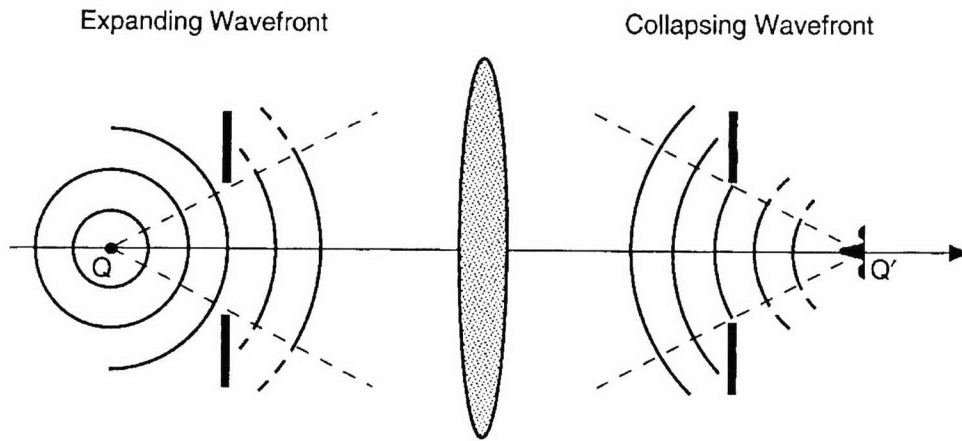


Figure 2-5: Example of an expanding (a) and collapsing (b) wavefront through an aperture (Reproduced from [28])

There are factors, however, that cause aberrations, even if the optical system, including the human eye, were perfect. The image of a point source through a circular pupil will still be distorted, that is, spread out across the retina as a diffraction pattern consisting of a bright central disk surrounded by faint, unevenly spaced concentric circles known as the Airy pattern [28]. The main reason for this phenomenon is that the wavefront emerging from the pupil is only a small portion of the complete wavefront needed to form a perfect point image [28].

In describing the wave nature of light, it is necessary to understand diffraction. But, diffraction problems are one of the most difficult problems encountered in optics [28]. Thus, it is easier to treat diffraction as a scalar phenomenon, the strength of which varies sinusoidally in time. Similarly, it is much easier to deal with images in a monochromatic form, rather than a polychromatic form.

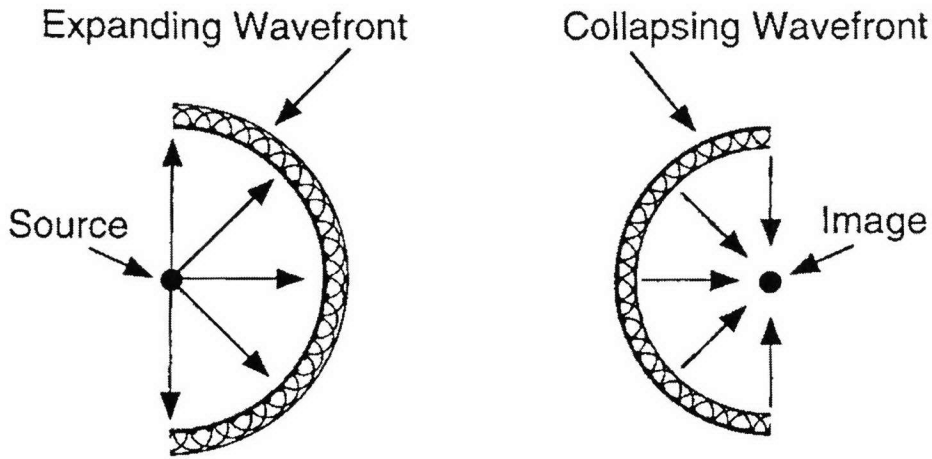


Figure 2-6: Huygens's theory of wavefront propagation (Reproduced from [28])

Thus, for a monochromatic wave, the field strength is given by

$$u(R, t) = M(R) \cos[2\pi\nu t + \phi(R)] \quad (2.8)$$

where $M(R)$ and $\phi(R)$ are the amplitude and phase, respectively of the wave at position R , while ν is the optical temporal frequency. For mathematical purposes, equation 2.8 can be rewritten as the real part of a complex exponential as follows:

$$u(R, t) = \text{Re}[U(R) \exp(-i2\pi \cdot \nu t)] \quad (2.9)$$

where i is the imaginary unit and $U(R)$ is a complex valued function of position only:

$$U(R) = M(R) \exp[-i\phi(R)] \quad (2.10)$$

The temporal oscillation of the field is not a major contributing factor to diffraction, thus the phasor $U(R)$ will be used as a description of the wavefront. Accordingly, the phasor description of Huygens's Wavelet is given by:

$$H(S, R) = \frac{1}{i\lambda} \cdot \frac{\exp(ikr)}{r} \cdot \cos\theta \quad (2.11)$$

where H is the complex amplitude of light at R due to Huygens's Wavelet at S, r is the radial distance from source point S to observation point R, k is $2\pi/\lambda$, wave number, which converts r to phase shift in radians, λ is the wavelength of light, and θ is the angle between line RS and the normal to the wavefront at S (see figure 2.7) [28], [12].

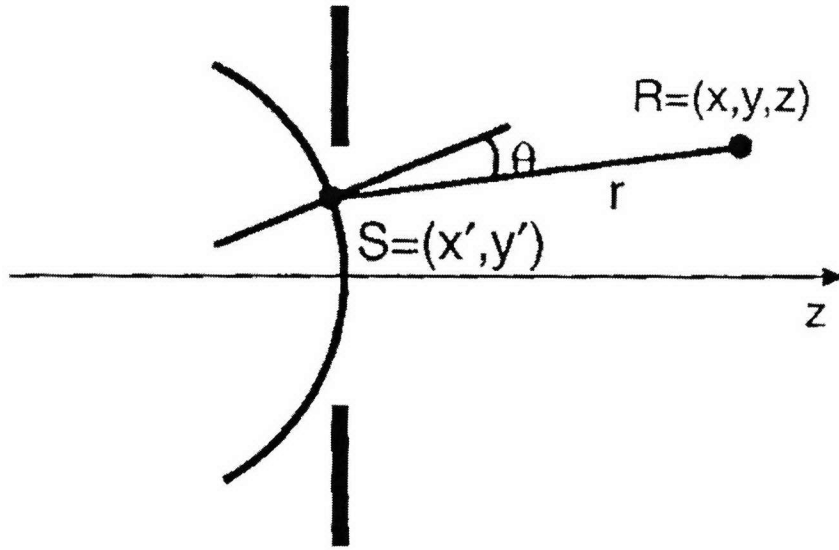


Figure 2-7: Geometry for computing the contribution of Huygens's wavelet at point S to the amplitude of light at point R (Reproduced from [28])

Equation 2.11 describes the secondary wavelet produced by a primary wavefront of unit amplitude. If the actual wavefront amplitude $U(S)$ is applied as a weighting factor, the wavelet at point S is the product of $U(S)$ and $H(S,R)$. The total field at R is found by applying the superposition principle to all of the fields due to the secondary wavelets. This results in a superposition integral over the entire aperture, A,

$$U(R) = \iint_{\text{Aperture}} U(S)H(S,R)dA. \quad (2.12)$$

Equation 2.12 is known as the Rayleigh-Sommerfeld diffraction integral [12].

2.3.3 Fourier Optics

The occurrence of equation 2.12 as a superposition resulting from the analysis of diffraction is due to the linearity of the system at hand [12]. Under certain conditions and restrictions, equation 2.12 reduces to a convolution integral, immediately allowing the application of the convolution theorem of Fourier analysis [5]. This “transforms the given quantities U and H into a corresponding pair of new quantities”. This is the domain of Fourier Optics [28].

In order to begin the analysis, a reference plane must be established between the aperture plane and the image plane. In reference to figure 2-7, the point R has the coordinates (x,y,z), and an arbitrary point in the aperture plane has the coordinates (x',y',0). Replacing z with the first two term of a binomial expansion of the Pythagorean Theorem describing z, the following approximation to the Huygens's wavelet can be made:

$$H(x',y',x,y,z) = \frac{1}{i \cdot \lambda \cdot z} \cdot \exp \left\{ i \cdot k \cdot \left(z + \frac{(x' - x)^2 + (y' - y)^2}{2z} \right) \right\} \quad (2.13)$$

This result leads to a further simplification of the Rayleigh-Sommerfeld diffraction integral [28]:

$$U(x,y) = C \iint_{Aperture} U(x',y') \exp \left(-\frac{ik}{z} (xx' + yy') \right) \cdot dx' dy' \quad (2.14)$$

where **C** is the complex constant

$$C = \frac{1}{i\lambda \cdot z} \exp \left\{ ik \left(z + \frac{x^2 + y^2}{2z} \right) \right\}. \quad (2.15)$$

Normalizing the (x,y) coordinates by substitution of variables $\hat{x} = x / \lambda z$ and $\hat{y} = y / \lambda z$, as well as a pupil function $P(x',y')$, which has a value of 1 inside the aperture and 0 outside, equation 2.14 becomes

$$U(\hat{x}, \hat{y}) = C \int_{-\infty-\infty}^{\infty} P(x',y') U(x',y') \exp\left[-2\pi \cdot i\left(\hat{x} x' + \hat{y} y'\right)\right] \cdot dx' dy'. \quad (2.16)$$

Except for the scaling factor C, “the Fraunhofer diffraction pattern is recognized as a two-dimensional inverse Fourier transform of the incident wavefront as truncated by the pupil function” [28].

Equation 2.16 can be summarized in compact form, where the arrow indicates the direction of the Fourier transform, by

$$U(\hat{x}, \hat{y}) \xrightarrow{F} P(\hat{x}, \hat{y}), \quad (2.17)$$

or in other words, that the amplitude U of the light distribution in a distant image plane due to diffraction of a monochromatic plane wave by an aperture is proportional to the inverse Fourier transform of the aperture’s pupil function. This brings into play a powerful tool of linear system analysis, the Fourier Transform [5], [12], [33]. Although this analysis seemingly focuses on diffraction, this can be easily applied to imaging systems by bringing into play the focusing properties of the lens through a generalization of the pupil function.

The pupil function a can be thought of as a two-dimensional filter, varying both amplitude and phase of each point on the emerging wavefront. This function captures the effect of the optical system without violating the assumptions that led to equation 2.17. It can be constructed as a complex valued function, made up of a product of two factors

$$P(x',y') = D(x',y') \exp(ikW(x',y')), \quad (2.18)$$

where $D(x',y')$ is attenuation factor, and $W(x',y')$ is a phase factor termed the wavefront aberration function. The wavefront aberration function is directly attributed to aberrations of the system [28]. Thus, the complex amplitude spread function $A(x,y)$ in the image plane, including the effects of diffraction, for a point source of light is equal to the inverse Fourier transform of the complex pupil function,

$$A(x,y) \xrightarrow{F} P(x',y'). \quad (2.19)$$

Most detectors of light, such as those found in the retina, are not able to respond fast enough to follow the rapid temporal oscillations of light amplitude. Consequently, these receptors respond to the intensity of light, which is real valued and defined as the “time average of the square modulus of the complex amplitude” [28], namely

$$I(x,y) = |A(x,y)|^2. \quad (2.20)$$

Thus, $I(x,y)$ is called the Intensity PSF. This characterization of the optical system of the eye will be central to the explanation of the proposed image pre-compensation mechanism.

2.4 Human Eye as an Imaging System

One of the major changes in the recent analysis of optical systems, and of course the human eye, is that any imaging system can be treated as a linear system characterized in the spatial domain by the PSF, regardless whether the image is focused, blurred, diffraction-limited or aberrated [33]. The underlying assumption is that the PSF is invariant to lateral translations of the point source. The PSF is thus said to be “space-invariant” [28].

The significance of this is that the retinal image of any object can then be computed with knowledge of the PSF and the spatial distribution of light intensities in the object.

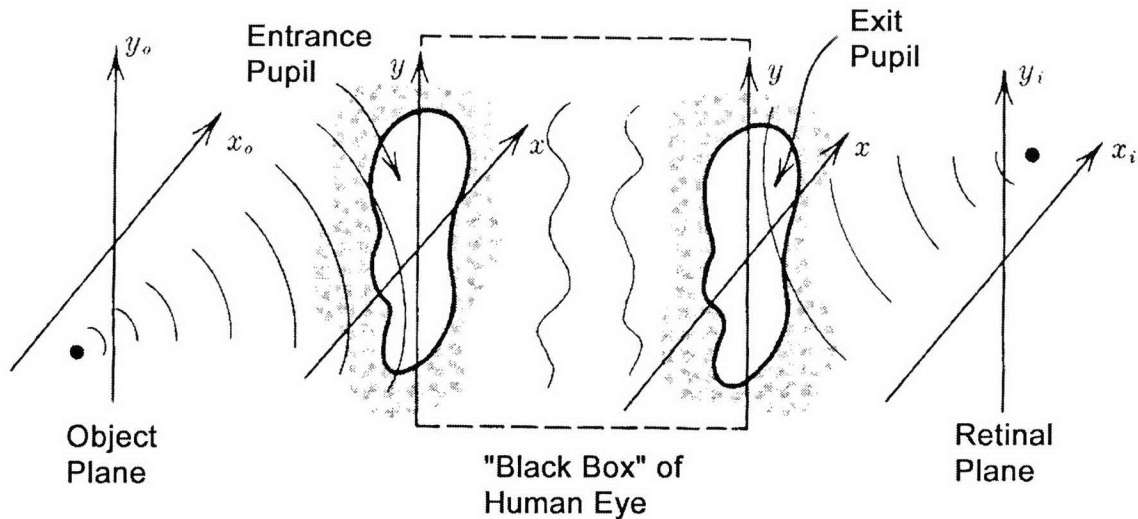


Figure 2-8: Black Box of the imaging process in the human eye (Modified from [12])

The resulting imaging process can be summarized by stating that the resulting retinal image is produced by the convolution of the system impulse response (i.e. the system PSF) with the object (i.e. the image predicted by geometric optics) [12], [28],

$$\text{spatial image} = \text{spatial object} * \text{PSF} \quad (2.21)$$

where $*$ denotes convolution.

In optics, the Optical Transfer Function (OTF) is one of the most useful descriptors of imaging performance of an optical system [25]. If this is true, then there should be a relationship between the OTF and the PSF, due to the fact that the PSF completely characterizes the optical system. There is such a relationship and it is, in fact,

established through the Fourier Transformation. Simply stated, the OTF is the complex valued Fourier transform of the PSF.

$$I(x, y) \xrightarrow{F} T(u, v) \quad (2.22)$$

According to the Convolution theorem of Fourier analysis, the convolution of two functions in one domain (either space or frequency) is the equivalent to the modulation or multiplication of the two functions in the other domain.

$$\text{image spectrum} = \text{object spectrum} \cdot \text{PSF} \quad (2.23)$$

This, through a series of manipulations, yields the following conclusions:

1. The intensity PSF is the inverse Fourier transform of the auto correlation of the pupil function

$$I(x, y) \xrightarrow{F} P(x', y') \star P(x', y') \quad (2.24)$$

where \star denotes correlation.

2. The OTF is the auto-correlation of the pupil function

$$T(u, v) = P(x', y') \star P(x', y') \quad (2.25)$$

Therefore, the relationship presented in equation 2.21 is verified.

When using the preceding arguments for practical applications, it is useful to first normalize the pupil coordinates by the pupil radius when formulating the analytical expression of the pupil function. Once the OTF is derived, the frequency scale may be converted into physical quantities by noting that the cutoff spatial frequency f_c set by diffraction is given by:

$$f_c = d / \lambda \text{ cycles per radian (subtended at the pupil center)} \quad (2.26)$$

where d is the pupil diameter and λ is the wavelength [28].

2.5 Wavefront Aberrations and Zernike Polynomials

The light entering a theoretically perfect eye, (i.e., defocus, aberration, and diffraction free), after being refracted and passing through the exit pupil, converges in the form of spherical wavefronts to a focal point on the retina [25]. Thus, all of the light arrives at this point in phase and maximum radiant energy is delivered to that point [33]. But, “diffraction is a fundamental property of the wave nature of light whenever it passes through an aperture” [25]. And since all optical systems have an aperture, it is impossible to build a diffraction free optical device. Even if the optics of the imaging system were perfect, the system would be at best “diffraction limited” [28].

When light passes through an optical system which contains aberrations, it will exit from the pupil as a wavefront that is aberrated from the ideal spherical surface, known as the ‘pupil sphere’.

For points that advance ahead of the pupil sphere, the sign of $W(x,y)$ is positive. For points that are retarded behind the pupil sphere, the sign is negative. This is the principle component of the pupil function, equation 2.17. Once the wavefront aberration function is known, the pupil function can be calculated. Applying the principles of Fourier optics to the pupil function, the derivation of the OTF and the PSF of the optical system is possible.

Most of the effort aimed at defining the pupil function of the eye has been directed towards measuring the wavefront aberration function [28]. According to optical theory, an analytical formula for the wavefront aberration may be synthesized using knowledge of the optical aberrations of the eye [18], [32].

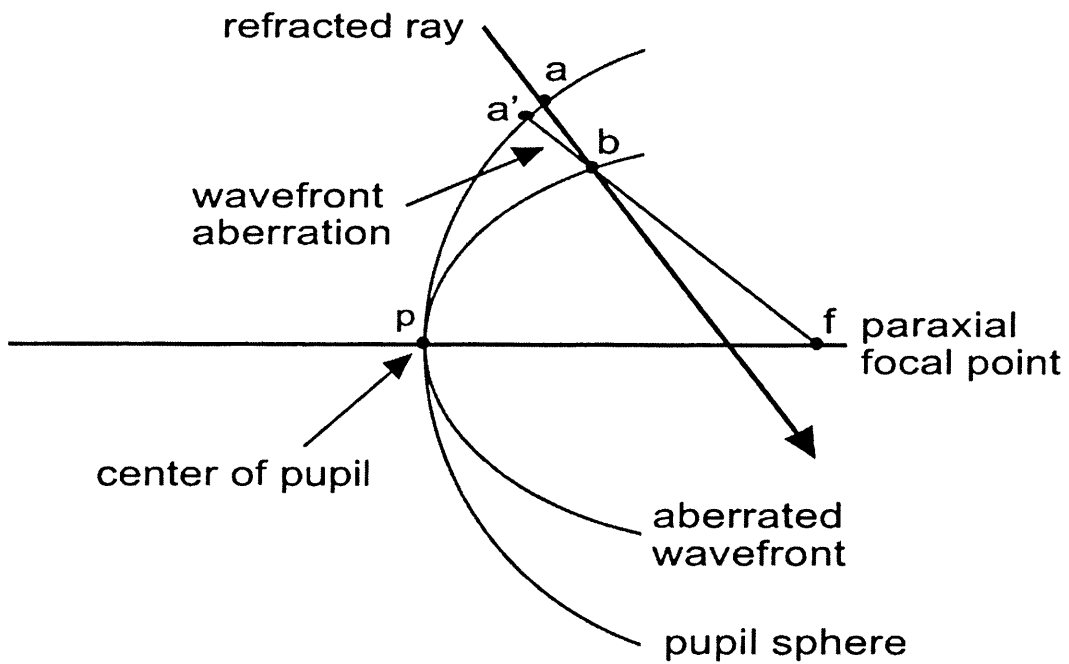


Figure 2-9: Wavefront aberration deviation from the pupil sphere; defined as either distance ab or $a'b$, depending on precise definition. For the range of the typical wavefront, these distances are essentially equal (reproduced from [25])

Liang et al. introduced a technique for measuring the wavefront aberrations of the human eye using a Hartmann-Shack sensor [21].

Once this data for the wavefront aberration is collected, it can be approximated by a polynomial expansion. One particular type of polynomial expansion, called the Zernike polynomial, is of particular interest. Zernike polynomials have been used in optical engineering for over 60 years [4], [22], [23]. The advantage of this polynomial series is that it is orthogonal over a circle for continuous curves, which is extremely beneficial for surface fitting and analysis [25], [30]. A detailed description is given by Born and Wolf [4], the scope of which is beyond this thesis.

2.6 Second Order Aberrations

Aberrations such as myopia, hyperopia, and astigmatism, are termed second order aberrations due to their Zernike polynomial descriptions [29] , [25]. An eye that is considered to be emmetropic (normal) bends parallel light rays from distant objects into sharp focus on the retina when the ciliary muscle is completely relaxed [13].

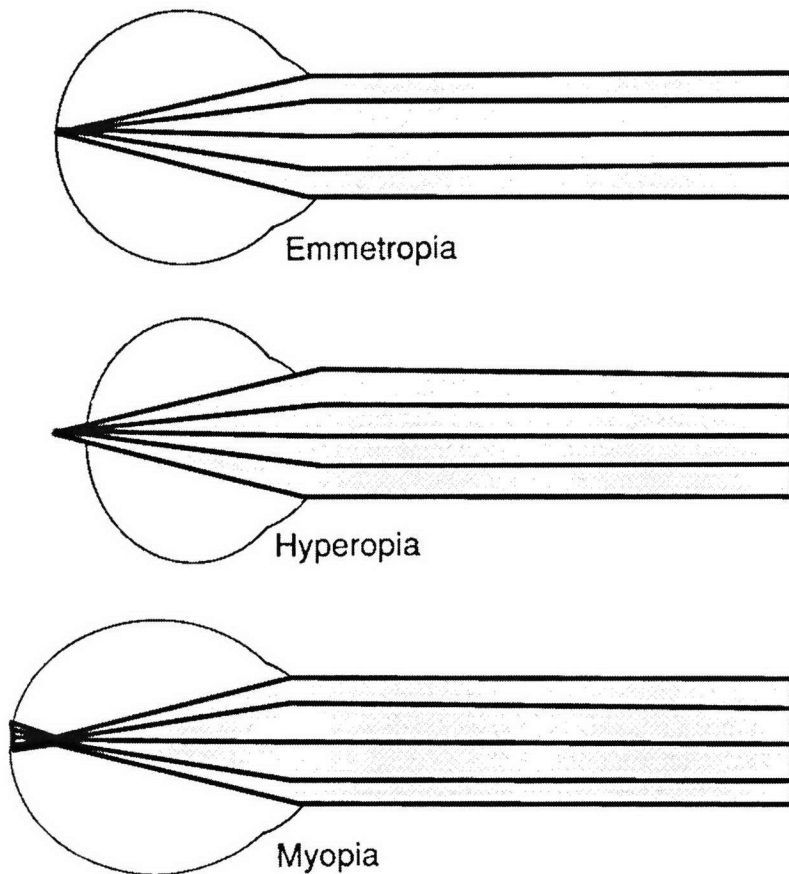


Figure 2-10: Parallel light rays focus on the retina in an emmetropic, behind the retina in an hyperopic eye, and in front of the retina for a myopic eye

Myopia and hyperopia, on the other hand, are both related to a spherical defocus, as shown in Figure 2-10. Similarly, an astigmatic eye focuses light from different planes at different focal distances, as shown in Figure 2-11.

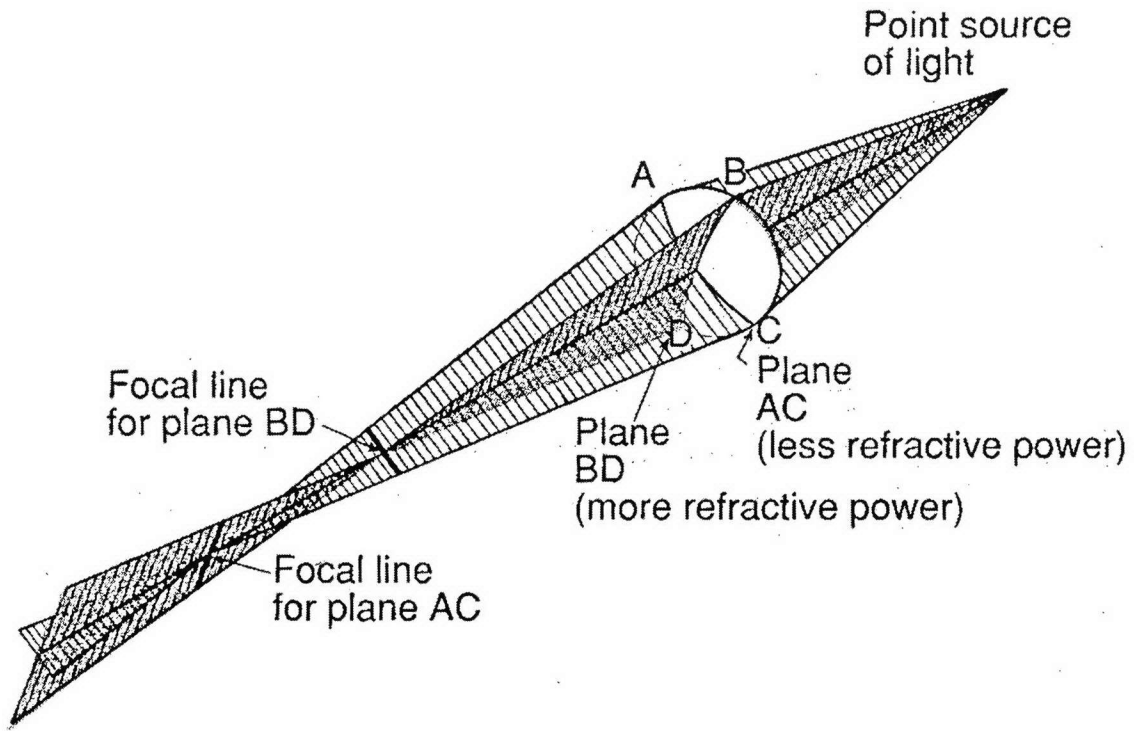


Figure 2-11: Demonstration of astigmatism. Light rays focus at one focal distance in one plane (AC), and at another focal distance in the plane at a right angle (BD).

2.6.1 Emmetropia

An emmetropic eye is again, an eye that does not suffer from any type of aberration. It has the ability to sharply focus objects on the retina. Figure 2-12 shows the wavefront aberration function of an emmetropic eye. As can be seen, there is no deviation of the exit wavefront from the ideal wavefront at any point within the pupil diameter. This is evident by the wavefront aberration having a value of zero across the pupil plane. The Zernike polynomial describing the wavefront aberration form hyperopia is:

$$W(x', y') = 0 \tag{2.27}$$

where x' and y' are units defined within the pupil plane.

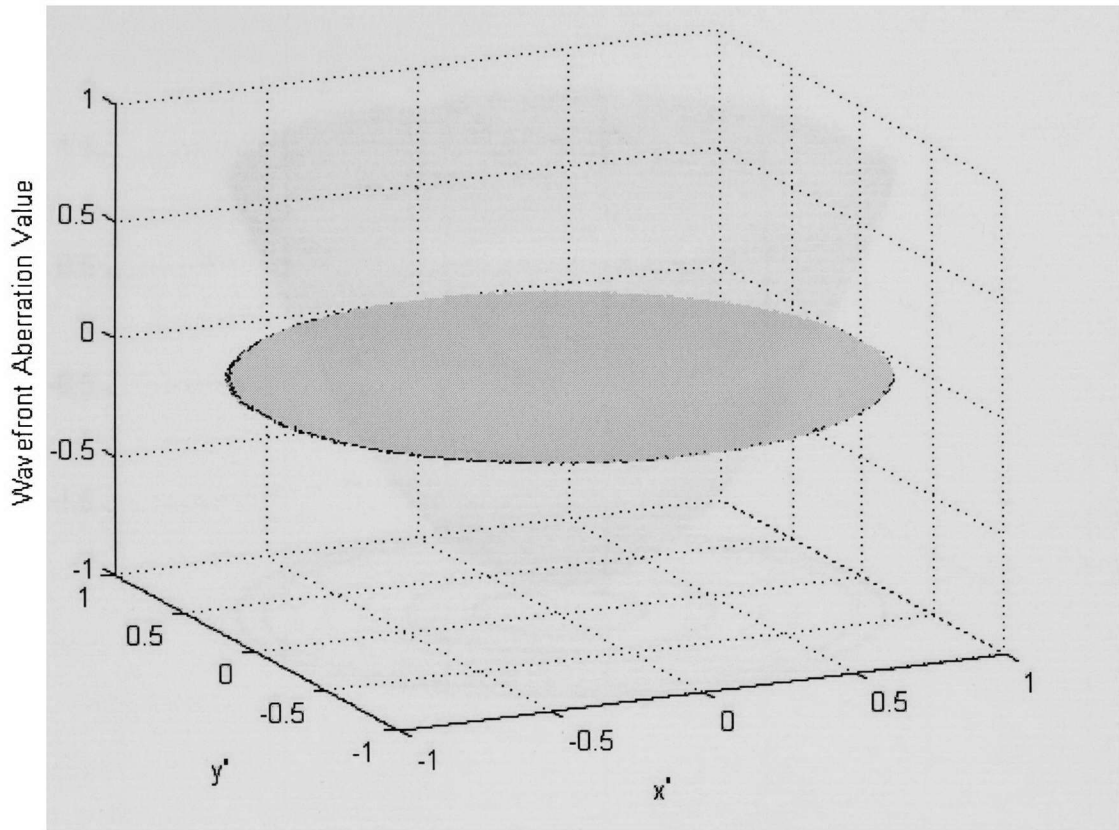


Figure 2-12: Example of the wavefront aberration for an Emmetropic Eye. Values are normalized over the pupil area. Notice that there is no deviation from 0 implying that the exiting wavefront did not suffer any type of distortion.

2.6.2 Hyperopia

A hyperopic eye does not possess the ability to focus images directly on the retina. In the unaccommodated state, the light rays are not bent sufficiently by the relaxed lens to come to a focus by the time they reach the retina. This is usually due to the eye being too short, or the lens having insufficient refractive power. The hyperopic eye can overcome this dilemma via accommodation if the ciliary muscles only have to contract a slight bit. If that is the case, there is still much refractive power left in the eye, enabling the focusing of close objects equally well [13]. This condition is also referred to as “far-sightedness”.

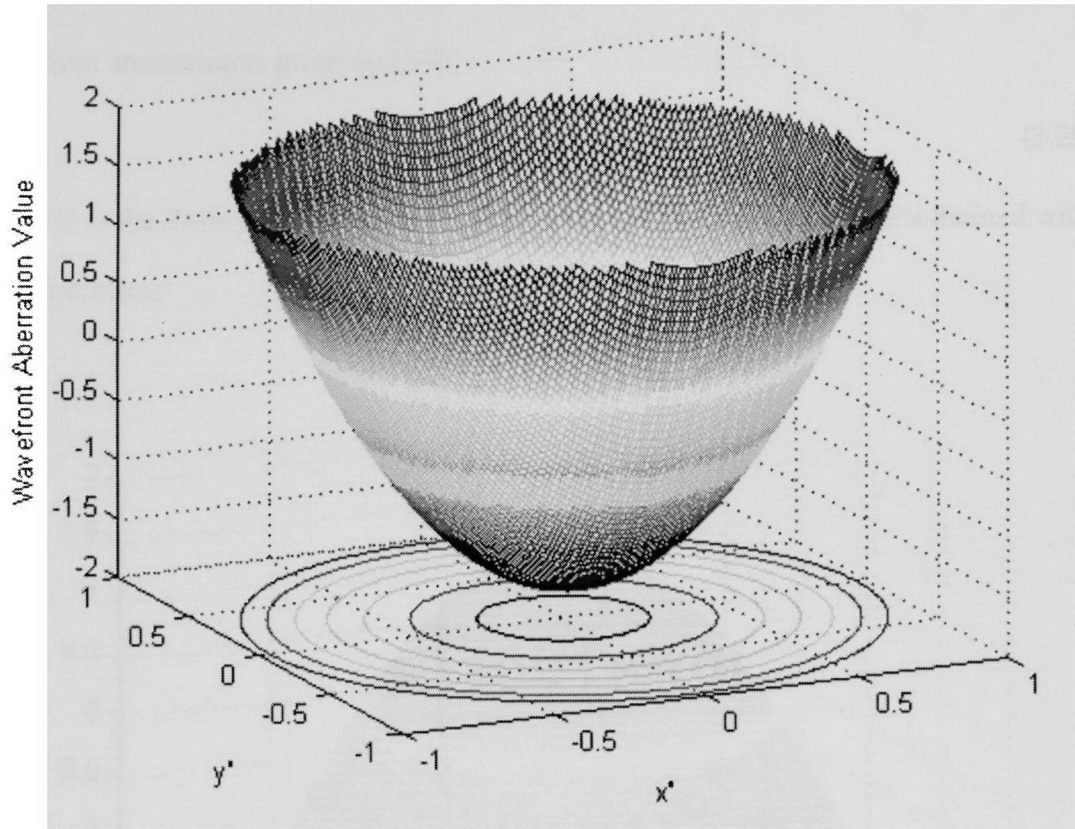


Figure 2-13: Example of the wavefront aberration for a hyperopic eye.

The Zernike polynomial describing the wavefront aberration form hyperopia is:

$$W(x', y') = Z[2(x'^2 + y'^2) - 1] \quad (2.28)$$

where Z is the Zernike coefficient or weight value, and x' and y' are units defined within the pupil plane.

2.6.3 Myopia

In the myopic eye, when the ciliary muscle is completely relaxed, the light rays from distant objects are focused in front of the retina, as can be seen in Figure 2-10. This is commonly due to the eye being too long, but can also result from the eye having too much refractive power. A person suffering from myopia has no method of focusing distant

objects, thus often being termed near-sighted. The Zernike polynomial describing the wavefront aberration is given by [25]:

$$W(x', y') = -Z[2((x')^2 + (y')^2) - 1] \quad (2.29)$$

where Z is the Zernike coefficient or weight value, and x' and y' are units defined within the pupil plane.

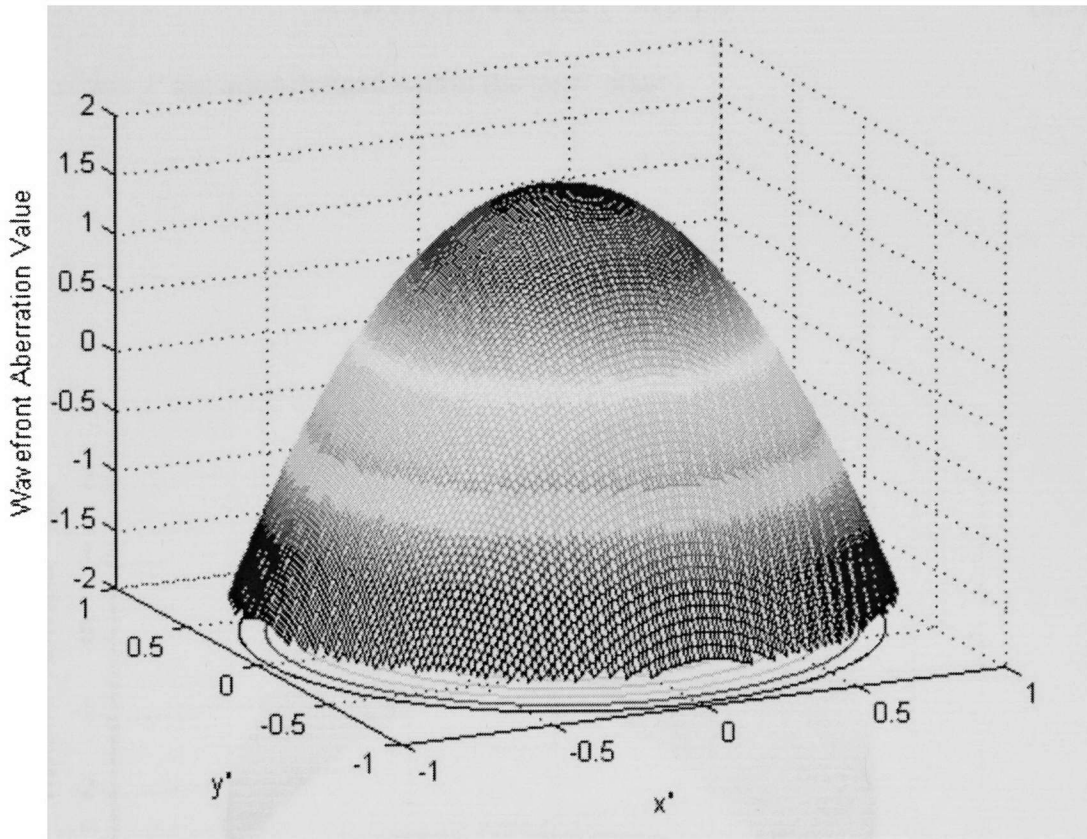


Figure 2-14: Example of the wavefront aberration for a myopic eye.

2.6.4 Astigmatism

Astigmatism is a refractive error of the eye that causes the visual image in one plane to focus at a different distance from that of the adjacent normal plane [13]. This is usually attributed from too great of a curvature of the cornea in one of its planes [13]. There are

two Zernike polynomials that describe the wavefront aberrations, in two directions. For a 45/135 astigmatic eye, the wavefront (Figure 2-15) aberration is [25]

$$W(x',y') = \sqrt{6}(2x'y'). \quad (2.30)$$

where x' and y' are units defined within the pupil plane.

For a 180/90 astigmatic eye, the wavefront (Figure 2-16) aberration is [25]

$$W(x',y') = \sqrt{6}((x')^2 - (y')^2) \quad (2.31)$$

where x' and y' are units defined within the pupil plane.

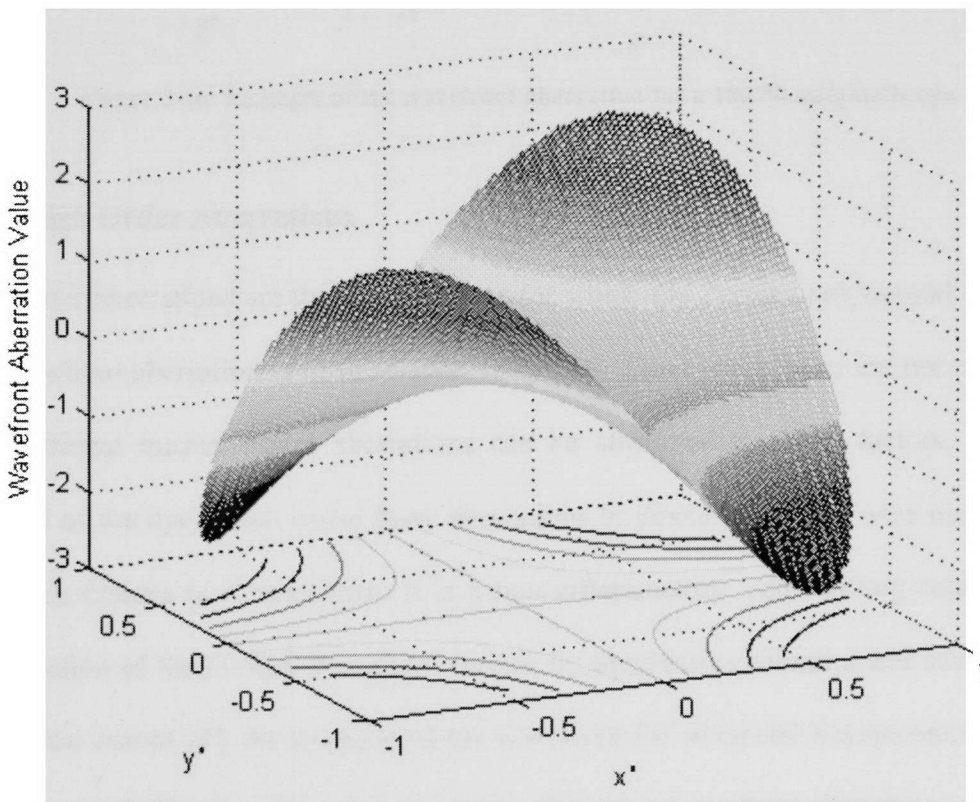


Figure 2-15: Example of the wavefront aberration for a 45/135 astigmatic eye.

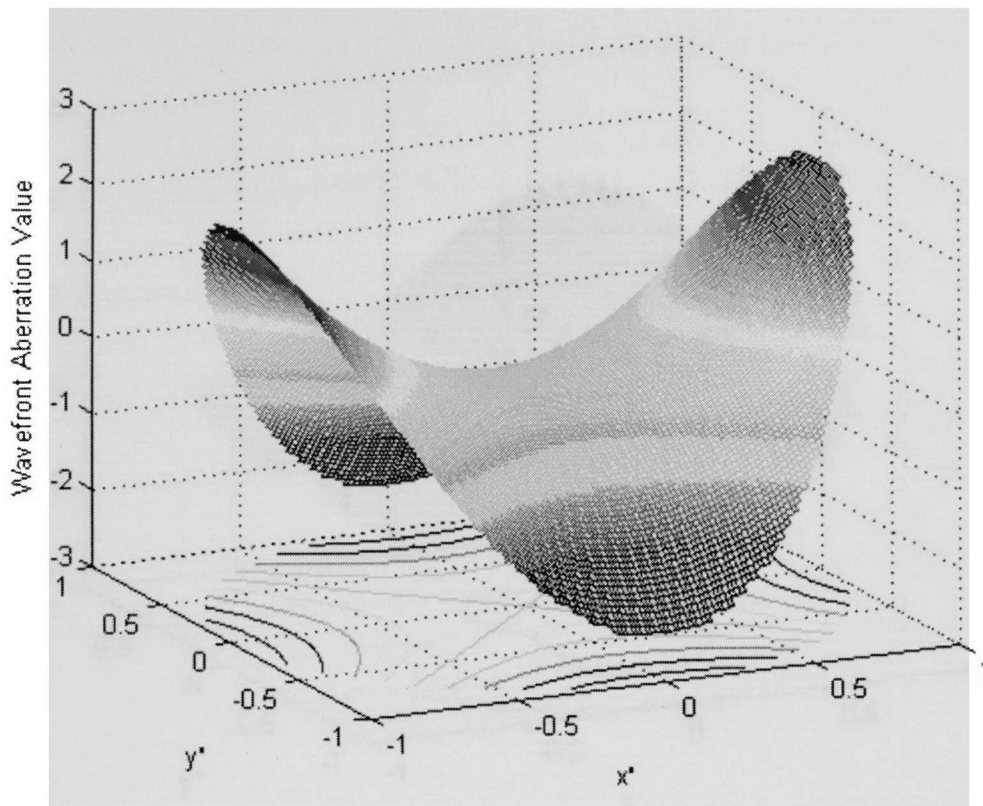


Figure 2-16: Example of the wavefront aberration for a 180/90 astigmatic eye.

2.7 High Order Aberrations

High order aberrations are those aberrations for which the Zernike polynomial describing the wavefront aberration is of third order or higher. These aberrations are not correctable by traditional means. These aberrations can be attributed to many factors, especially diseases of the eye which cause these aberrations to develop in other wise normal eyes. One such disease is Keratoconus. It is a non-inflammatory, self-limiting ectasia of the axial portion of the cornea. It is characterized by progressive thinning and steepening of the central cornea [7]. An example of the wavefront for advanced Keratoconus is shown in Figure 2-17. The Zernike polynomial describing this wavefront aberration is of eighth order and was obtained from [6].

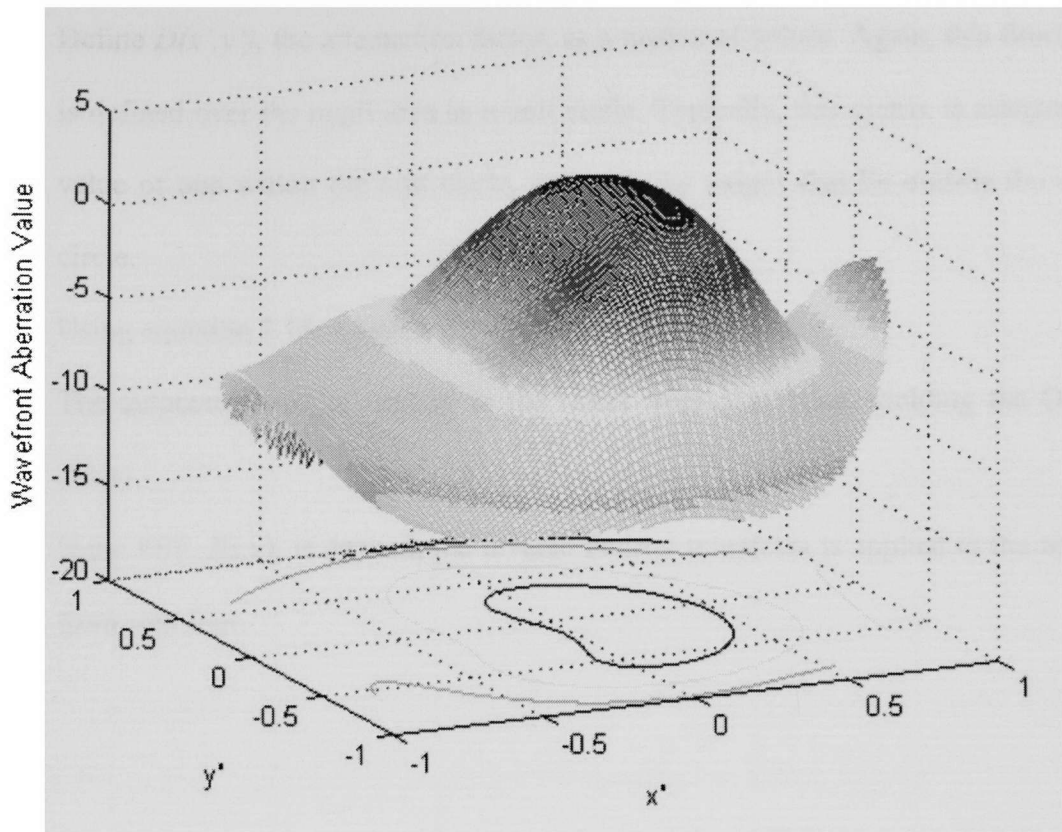


Figure 2-17: Example of the wavefront aberration for a real eye, suffering from advanced Keratoconus.

2.8 Obtaining the Analytical PSF

In order to obtain an analytical model of the PSF, or similarly the OTF, the following steps must be followed:

1. Formulate a matrix of values generated from the wavefront aberration function, $W(x',y')$, defined over the pupil area. The units of this function are normalized for ease of calculation. Thus the pupil area can be considered a unit circle for the purposes of calculations. Values of the matrix that lie outside the unit circle are made to be zero. An example of a wavefront aberration function is given by equation 2.28.

2. Define $D(x',y')$, the attenuation factor, as a matrix of values. Again, this function is defined over the pupil area as a unit circle. Typically, this matrix is assigned a value of one within the unit circle, and zero for values that lie outside the unit circle.
3. Using equation 2.18, a matrix for $P(x',y')$, is generated.
4. The autocorrelation is applied to the result from step three, yielding the OTF, $T(u,v)$.
5. If the PSF, $I(x,y)$, is desired, the inverse Fourier transform is applied to the result from step four.

3 CLINICAL VISUAL OPTICS

The interpretation of images is typically characterized by ambiguity, making it extremely difficult to quantify any research on human vision. The ability with which human beings can extract information from an image is due to many factors, some of which cannot be quantitatively measured, such as the thought process behind identification of patterns. One approach to overcoming the challenges presented by such factors has been to “define the visual capability of an individual in terms of the metrics derived from an understanding of how individuals perceive spatial information” [20].

“Selective Filtering”, a model of human vision that is based on “the selection and processing of certain types of visual information and the suppression of others” [20], is particularly useful, even though it only provides an initial explanation of how humans detect and recognize images. The quantification is approached from the standpoint of contrast sensitivity and the filtering properties of the observer are presented in terms of how they can be quantified through contrast sensitivity measurements obtained with a vision chart.

3.1 Visual Acuity

Visual acuity refers to the ability of a human being to clearly see high contrast spatial information in an image [20]. The visual acuity can be limited by optical blur introduced by wavefront aberrations, light scatter due to media opacities of the lens, or by loss of neural sensitivity in retina. This thesis concerns itself with the first of these limitations, namely the limitations introduced by the wavefront aberrations in the eye. Another factor to consider is the increased coarseness of retinal sampling towards the periphery of the

eye, compared with that of the fovea [20]. Thus for the purposes of this thesis, only images that project onto the foveal region of the retina, or in other words, that are directly on the visual axis, will be considered.

Visual acuity is generally measured by having the observer detect and identify high contrast targets of different sizes placed at a prescribed distance [20]. In 1862, the creation of the Snellen visual acuity chart (see figure 3.1) has been the cornerstone of visual assessment.

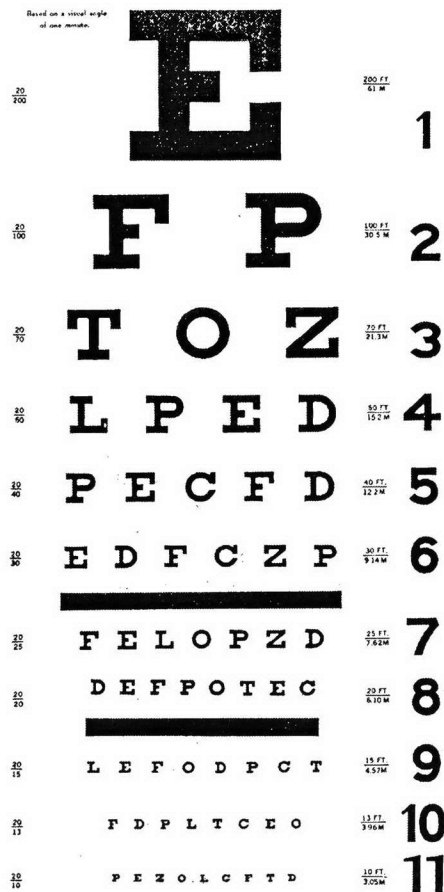


Figure 3-1: The Snellen visual acuity test chart

This thesis takes advantage of the fact that a Snellen type of visual acuity is an “acceptable measure of the optical quality of the eye in the sense of how well an image is focused” [20].

3.2 Eye Chart Descriptions

“The longstanding acceptance of the Snellen chart, and the need to create vision standards for the military in World War I, are responsible for the contemporary notion that a result of ‘20/20’ with the Snellen chart denotes good vision” [20]. The typical Snellen chart, shown in figure 3-1, is composed of eleven lines containing letters, varying in quantity from one letter on the first line, to 9 on the eleventh line. Snellen assumed that a letter, suppose for example, the capital letter E, “could just be seen by the average corrected eye if the thickness of the limbs and of the spaces between them subtended one minute of arc at the eye. The angular subtense of such a letter would therefore be five minutes of arc vertically and four to six minutes horizontally, depending on the style of type and the particular letter of the alphabet” [3].

The Snellen chart suffers from some fundamental limitations for the evaluation of functional vision. Some of these are:

1. There is a different number of letters per line. Therefore, allowing one or two mistakes per line has a different meaning.
2. There is no regular progression in letter size, which makes reporting a loss of two lines of vision misleading.
3. Various Snellen letters differ in perceptual difficulty. Different lines do not have letters of equal difficulty.

4. Test luminance conditions are not standardized for use with the Snellen acuity chart.

Thus, it was not until 1976, when Australian optometrists Bailey and Lovie proposed a new visual acuity test, overcoming most of the difficulties of the original Snellen chart [3]. They provided a new design for eye charts that relies on two fundamental principles [1]:

1. The test task is the same at each level so that the angular size remains as the only measure of visual acuity
2. The letter size progression is in uniform steps on a logarithmic scale so that the scaling factor is constant throughout the chart and will remain unaltered when non-standard viewing distances are used

Bailey and Lovie chose to express the measure of visual acuity in terms of “the logarithm of the angular limb width (in minutes of arc) of the smallest letters recognized at 6 meters” [3]. This notation is called the ‘logMAR’, standing for the logarithm of the minimum angle of resolution. The specifications of the chart are as follows [1]:

1. Legibility. All of the letters on each line are equally legible.
2. Number of letters. Each row has an equal number of five letters.
3. Letter Spacing. The spacing between each letter is one letter width.
4. Row Spacing. The spacing between rows is equal to the height of the letters in the smaller row.
5. Size progression. The progression of letter sizes follows a geometric progression ratio of equal to 1.2589.

6. Range of sizes. The chart is designed for a standard testing distance of six meters. At this distance, the largest letter subtends 10 minutes of arc, and the smallest subtends 0.5 minutes of arc.
7. Scale notation. The rows of the chart are labeled with visual acuity ratings that relate to the standard viewing distance of six meters. On one side, the visual acuity ratings are given in logMAR units. On the other side, the visual acuity is given in the Snellen form.

Table 3-1 shows the relationships between logMAR steps, angular size of detail and Corresponding distance acuities. An example of a Bailey-Lovie chart is shown in figure 3-2.

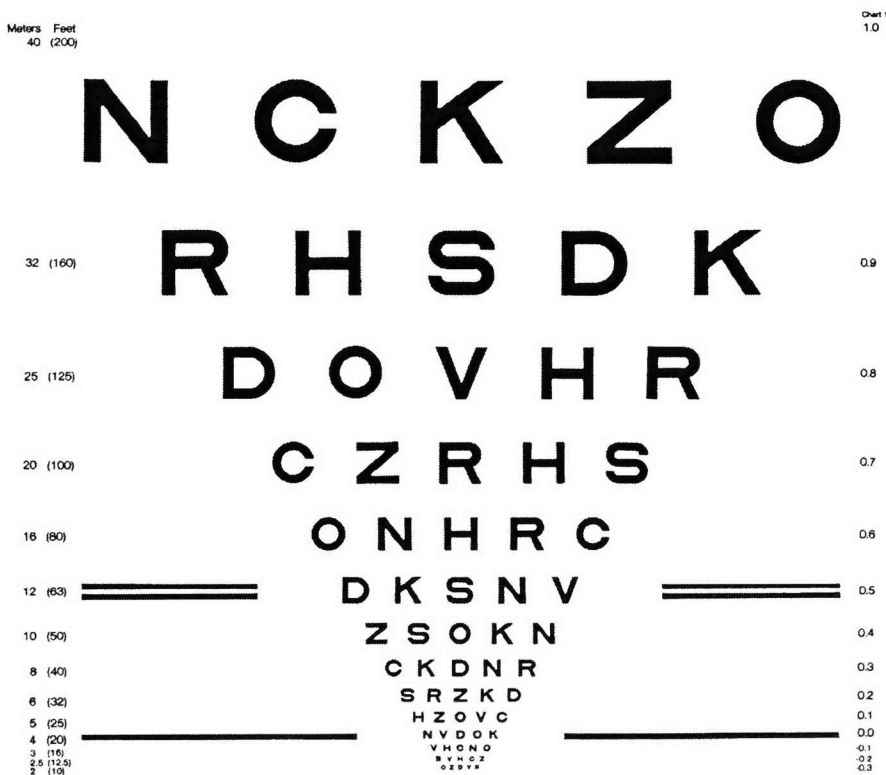


Figure 3-2: An example of a Bailey-Lovie logMAR eye test chart using 'Sloan' letters

Additionally, the Bailey-Lovie charts available for use in the United States, are produced using letters, called ‘Sloan’ letters, that are of 5x5 non-serif format, of similar legibility, and are scaled down to be used at four meters, as stipulated by the Committee on Vision of the National Academy of Sciences – National Research Council [3].

Table 3-1: The log of the Minimum Angle Resolved (logMAR) scale, corresponding minimum angles of resolution, and equivalent decimal V and Snellen distance acuities

logMAR steps	Angular Size of detail (in minutes of arc)	Corresponding distance acuities		
		Decimal V	at 6m (denominator of Snellen Fraction)	at 20ft (denominator of Snellen Fraction)
1.3	20	0.05	120	400
1.2	15.9	0.063	95	320
1.1	12.7	0.079	75	250
1	10	0.1	60	200
0.9	7.9	0.126	48	160
0.8	6.3	0.158	38	125
0.7	5	0.2	30	100
0.6	4	0.251	24	80
0.5	3.2	0.316	19	63
0.4	2.5	0.398	15	50
0.3	2	0.501	12	40
0.2	1.6	0.631	9.5	32
0.1	1.3	0.794	7.5	25
0	1	1	6	20
-0.1	0.8	1.259	4.75	16
-0.2	0.6	1.585	3.75	12.5
-0.3	0.5	1.995	3	10

3.3 Evaluation of Visual Performance

The human eye is capable of several tasks involving all of the complexities of vision.

These tasks can be classified under the following:

1. Light Perception
2. Discrimination
3. Form Vision and Recognition

4. Resolution
5. Localization
6. Higher tasks where the visual system stimulates other responses

The two most important of these aspects in clinical work are those of form vision and resolution [3]. If the eye views a large letter such that the size of the letter is proportionally large with respect to the retinal receptors, “it is the general shape of the letter which has to be recognized, no matter whether the retinal image is sharp or blurred” [3].

Used in conjunction with a suitable scoring system, the logMAR charts are better suited for research and statistical analysis than the conventional letter charts used in refraction [3], such as the Snellen chart.

As logMAR values decrease with letter size, as seen in table 3-1, the scoring systems and calculation of the corresponding visual acuity can be complicated [3]. The basic problem is related to the difference between the arithmetic mean and the geometric mean for a set of numbers [17]. As shown in table 3-1, the letters on each line follow a geometric progression. In other words, they change in a uniform step on a logarithmic scale. Thus, any acceptable statistical analysis, such as mean, standard deviation, or variance, must be done first using the logMAR values, and then converting into a visual distance acuity score. This can be accomplished using the following equations [17]:

$$\log MAR = -\log(V) \quad (3.1)$$

where V is the decimal acuity. This decimal acuity can be converted back into the Snellen equivalent by

$$\text{denominator of Snellen} = 20/V . \quad (3.2)$$

For example, to average two scores of 20/20 and 20/200, first convert to decimal, $20/20 = 1.0$ and $20/200 = 0.1$. Now, this is converted to logMAR by taking the negative logarithm, $\log(-1) = 0.0$ and $\log(-0.1) = +1.0$. The average of 0.0 and 1.0 is 0.5. Converting back from logMAR value of 0.5, the corresponding visual acuity score is 20/63, the correct geometric average.

The score for an eye exam is usually found by number of letters the person read correctly. Although recording the last line that was completely read, or if the person reads at least up to a threshold, three out of the five letters counting as a complete line, is acceptable, it tends to reduce the precision measurement [17].

Holladay proposes a method that is “more accurate” in that it interpolates between the values of the logMAR acuity using the fraction of the numbers read correctly on a visual acuity line. For instance, suppose the acuity eye test chart of a Bailey-Lovie type. Thus, there are five letters on each line. Suppose a person taking the eye test read all of the letters on the 20/50 line (corresponding to a logMAR value of +0.4) and only three of the five letters on the 20/40 line (corresponding to a logMAR value of +0.3). Three-fifths of the way from logMAR 0.4 to logMAR 0.3 is logMAR 0.34. This can be found by the following equation:

$$tLV = cLV - 0.1(n/5) \quad (3.3)$$

where tLV is the true logMAR value, cLV is the logMAR value for the last line completely read, and n is the number of letters read correctly on the subsequent line.

Once the true logMAR value is determined, the visual efficiency can then be determined. In 1925, the American Medical Association (AMA) adopted a visual efficiency scale based on the work of Snell, and Scott Sterling [3]. This is based on a

mathematical relationship whereby the visual efficiency E decreases logarithmically as the minimum angular detail size A or the letter size D increases arithmetically.

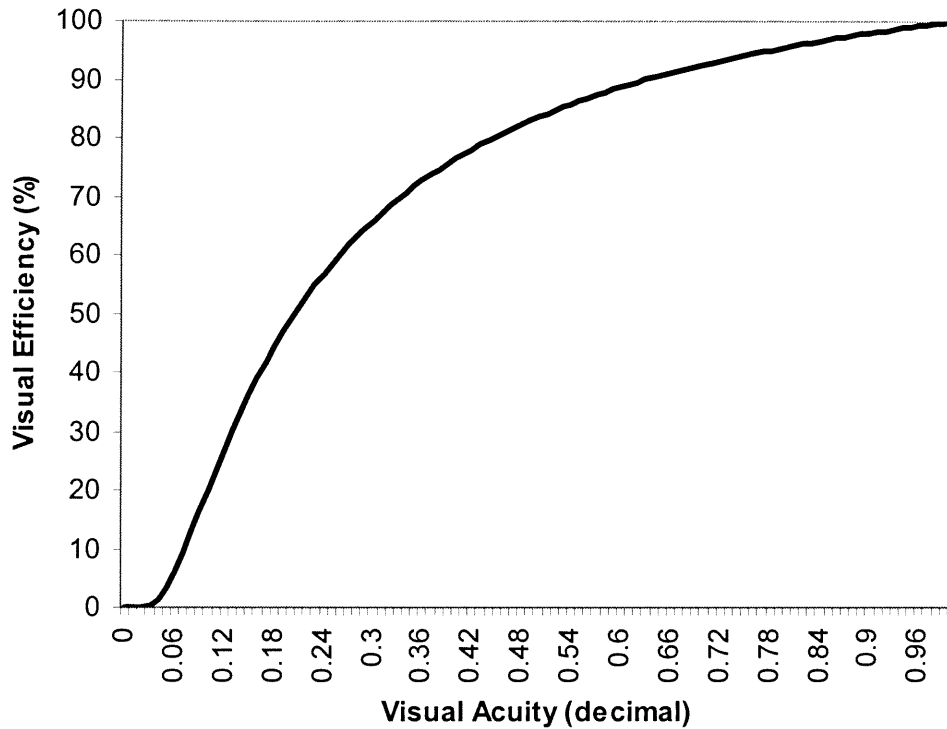


Figure 3-3: Relationship between AMA visual efficiency, and Snellen visual distance acuity in decimal

According to the study done by Sterling, the experimental results for determining the visual efficiency (E) yield the following equations [3]:

$$\log E = -0.0777 A + 2.0777, \quad (3.4)$$

$$A = \frac{2.0777 - \log E}{0.0777}, \quad (3.5)$$

and

$$V = 1 / A, \quad (3.6)$$

where V is the decimal visual acuity obtained from the Snellen distance acuity. A plot of the Visual Efficiency versus the Visual acuity is shown in figure 3-3.

4 DECONVOLUTION

In order to provide the pre-compensation of the wavefront aberration function, a method for the transformation of the image to be displayed is necessary. In order to provide the foundation for obtaining this pre-compensation for the eye, the optical system of the eye is assumed to be linear and shift invariant. For any linear-shift invariant system, the impulse response completely characterizes the system [15]. Similarly, the optical system of the human eye is characterized by its PSF. If the input to the optical system is a weighted super-position of spatially shifted impulses, then the output is a weighted superposition of the system response to each spatially shifted impulse [15]. This weighted superposition is termed the convolution sum for discrete systems or the convolution integral for continuous systems. This thesis makes use of this principle, as a digital image can be considered a discrete, finite, superposition of weighted impulses, each ranging in weight from 0 to 255.

Assuming the output is given by convolution, the reverse process is called deconvolution. Traditional deconvolution uses knowledge of the impulse response to restore, or recover the input to a system, given the distorted output. This thesis proposes to use deconvolution, not on the final distorted image to restore the original, but instead to pre-deconvolve the intended image. Once this deconvolution is done on the image, if the image is viewed through the optical system (i.e. the image is implicitly convolved with the PSF of the optical system), the output (or the retinal image) should resemble the input to the entire process.

Thus, it is necessary to implement a method of deconvolution that adheres to the following:

1. The deconvolution must yield non-negative results.
2. The result of the deconvolution is in the range from 0 to 255.

In order to satisfy this, this thesis explored three deconvolution methods: Van Cittert's, Non-negative least squares, and finally Minimum Mean Squared Error filtering. A brief explanation of the first two methods will be given in addition to a detailed explanation of the final method. The first two methods did not yield desirable results, even though they are positively constrained. The third, in contrast, yields negative results, but it was found that they can be post-processed to effectively display usable approximations of the pre-compensated images on the computer screen. Thus the last method, the minimum mean square error filtering was used as the preferred method deconvolution for this project.

4.1 Van Cittert's Method

The Van Cittert's method of deconvolution has been applied to many forms of restoration, from Azimuth-Doppler radar images [2] to images from the Hubble telescope [10]. This method works in an iterative fashion with successive substitutions of the input image to the system. The error between the actual image and the approximation to the image helps drive the algorithm towards a better approximation after each iteration [5]. Letting \otimes denote convolution, the deconvolution can be summarized by the following equations. Assume that the output, Y_N , is given by the convolution of the input, X_N , with the PSF, H_N :

$$Y_N = X_N * H_N \quad (4.1)$$

where $*$ denotes convolution.

The deconvolution iteration can then be written:

$$XN_o = \lambda \cdot YN \quad (4.2)$$

$$XN_{k+1} = \lambda \cdot YN + XN_k - \lambda \cdot C[XN_k \otimes HN] \quad (4.3)$$

where λ is the factor controlling the rate of convergence, and C is a constraint. For the case of a digital image, the constraint is that the values within the constraint operator are all positive and less than or equal to 255.

This method, when applied to the problem that concerns this thesis, produced results that were both positive and less than 255, but did not implement the exact solution of the inverse. The mean squared errors present in the solutions found through this method were typically larger than suitable for the intended application.

4.2 Non-Negative Least Squares

The convolution problem from which the Non-Negative Least Squares (NNLS) deconvolution algorithm is derived can be rewritten in the following form in the presence of noise:

$$yn(x, y) = H(x, y) * xn(x, y) + n(x, y) \quad (4.4)$$

where $xn(x,y)$ is the input to the optical system, $yn(x,y)$ is the output of the optical system, which in the case of the human eye is the retinal image, $H(x,y)$ is the PSF, and $n(x,y)$ is additive noise. Similarly, we can write equation 4.4 in vector matrix form, as follows:

$$\mathbf{yn} = \mathbf{H} \cdot \mathbf{xn} + \mathbf{n} \quad (4.5)$$

Suppose that $yn(x,y)$ is of size $M \times N$. The first N elements of vector \mathbf{yn} can be formed by using the image elements in the first row of $yn(x,y)$, the next N elements from

the second row, and so on. The result is an $MN \times 1$ size matrix. This process of row scanning to create \mathbf{xn} is used to create \mathbf{xn} and \mathbf{n} . The matrix H has the dimensions $MN \times MN$. A description of how H is formed is given in [2].

From equation 4.5, it would seem that solution to the deconvolution is reduced to simple matrix manipulations. This is not the case, however. Most digital displays are at least of size $M=800$ and $N=600$. Letting $N=0$, the vectors, Y_N , and X_N are of size 480000×1 , and H is of size 480000×480000 . Manipulation of matrices this size is not an easy task. Furthermore even for small images, this method does not yield good visual results, even though it does minimize the norm, $|\mathbf{H} \cdot \mathbf{xn} - \mathbf{yn}|$, [11].

4.3 Minimum Mean Square Error Filtering

Minimum Mean Square Error filtering incorporates statistical information about the noise, as well as knowledge of the degradation function (PSF) [11]. This method is founded on considering images and noise as random processes and the objective is to obtain an estimate of the uncorrupted image such that the mean square error between the estimate and the true uncorrupted image is minimized [11]. The error measured is given by:

$$e^2 = E \left\{ \left(XN - \hat{XN} \right)^2 \right\} \quad (4.6)$$

where $E\{\cdot\}$ is the expected value of the argument [11]. It is assumed that the noise and the image are uncorrelated; that one or the other has zero mean; and that the gray levels in the estimate are a linear function of the levels of the degraded image. Thus, based on

these assumptions, the minimum of the error function in equation 4.6 is given in the frequency domain by

$$\hat{X} = \left[\frac{1}{H} \frac{|H|^2}{|H|^2 + S_n / S_x} \right] Y \quad (4.7)$$

where H is the PSF, X is the estimate of the deconvolution, Y is the degraded image, S_n is the power spectrum of the noise, and S_x is the power spectrum of the true result of deconvolution [11]. Since that power spectrum of the image and the noise are seldom known, the following can be used to approximate equation 4.7 [11]:

$$\hat{X} = \left[\frac{1}{H} \frac{|H|^2}{|H|^2 + K} \right] Y \quad (4.8)$$

where K can be varied to achieve the best visual result.

The factor K in equation 4.8 is used as a substitution for the ratio of the power spectrum of the noise to the power spectrum of the undistorted image. As K approaches zero, the minimum mean square error filter approximates the ideal inverse filter,

$$\hat{X} = \frac{Y}{H}, \quad (4.9)$$

to a greater degree of accuracy. This accuracy is reflected in the display ability of the image on a monitor. For higher values of K, the pre-compensated image is more displayable, in that the values in the image do not swing very far past 255 or very far below 0. On the other hand, since the inverse process is closer the ideal case as values of K decrease, the retinal image, resulting from viewing the pre-compensated image through the aberration, is closer to the intended image but lacks the display ability, having values the swing very high both positively and negatively. Thus, there exists a trade-off between

display ability and how closely the minimum mean square error filter realizes the desired pre-compensation. Keeping this in mind, the value of K can be varied until desirable results for the pre-compensation are obtained.

5 EXPERIMENT DESCRIPTION

5.1 Overview

Quantification of the results was done with the participation of human subjects. The Institutional Review Board approval for the experimental evaluation and supporting documents can be found in the appendix. In order to proceed with the testing of this method, human subjects having a satisfactory standard visual acuity of 20/20 [3], either corrected or natural, were recruited. Then, a refractive error, specifically defocus, was artificially induced by means of a pre-selected lens. A similar procedure was used by Sonksen to test visual function [26].

In order to provide a well-known and standardized method of reporting visual performance, a standard Eye Test Chart was used. Since this thesis proposes a digital approach to the pre-compensation, the images that will be used must be digital, implying that the Eye Test Chart must be digital as well. It was decided that the type of chart to be used is a Bailey-Lovie visual acuity chart with 'Sloan' letters, (Figure 1-5). This chart overcomes most of the problems of traditional eye charts [1], [3]. Additionally, once the visual acuity is assessed, statistical calculations, such as mean, standard deviation, and variance, can be made using this type of chart [17].

The experiment consisted of three parts:

1. A visual acuity assessment with the un-compensated chart images (Figure 5-17 (a)), using the right and left eye independently.

2. A visual acuity assessment with the un-compensated chart images but introducing a controlled defocus refractive error (see Figure 5-17(b)), using the right and left eye independently.
3. A visual acuity assessment with the compensated chart images using the method presented, viewed through the induced refractive error (see Figure 5-17(c)), using the right and left eye independently.

The method of displaying the images to the subjects was through the use of the SONY Mavica Digital Camera. The camera was resting on a tripod, pointing at the digital display and adjusted such that the camera only captured the area of the digital display. This camera has a digital LCD display behind it, allowing for the subjects to sit directly behind the camera, at the required distance for the visual acuity test (for the purposes of this test, the distance was two meters). This introduced an intervention in the imaging process, whereby the image is displayed on the digital display is captured by the digital camera, and then displayed to the subject through the camera's LCD. Using this setup, the refractive error can be introduced through the use of a lens. This method of displaying the images through the digital camera was preferred over having the subject directly looking at the digital monitor because of the eye's inherent ability to accommodate. Accommodation results from the human eye trying to bring the image into focus. It was found, that even with the worst spherical lens available, in terms of its defocusing capability, the eye would attempt to accommodate and focus the images. The digital camera, on the other hand, can be set to a fixed focus, allowing for the introduction of a defocus without any problems. A -6.0 spherical prescription optical lens was used to introduce the refractive error. When the lens is placed in front of the camera, and the auto

focus of the camera is turned off, the images of the eye test chart shown to the user will be defocused, thus allowing for testing of the pre-compensation method.

5.2 System Elements

The main elements used to test the proposed method are as follows: A personal computer, being the main platform for the digital implementation of the deconvolution, the computer monitor, providing a visual display of the eye chart, and pre-compensated eye chart, the SONY Mavica Digital Camera, in a sense acting as a simulated eye, and the lens, introducing the optical aberration.

5.2.1 Monitor

The digital display chosen to be used for the testing of the pre-compensations was a Gateway VX1120, 22-inch flat-screen monitor shown in Figure 5-1.



Figure 5-1: Gateway VX1120 22-inch Monitor showing the third line of ETDRS Eye Test Chart

This monitor was chosen due to its size and display resolution. Evidently in order to implement an a suitable test bed using the concept of an eye chart test, the eye chart must be represented with accuracy, high resolution, and in true size on the digital display. Thus, the largest monitor with the highest resolution available was chosen. The detailed specifications of the monitor are shown in table 5-1.

Table 5-1: Gateway VX1120 Digital Monitor Specifications [8]

CRT	55-centimeters (cm) diagonal (51-cm inches viewable) flat face color CRT, anti-reflective, anti-static, 90 ° deflection, 0.24mm dot pitch CRT
Resolution	2048 × 1536 maximum
Display colors	Unlimited
Scanning frequency	Horizontal, 30 to 69KHz; Vertical, 50 to 110 Hz
Display area	284 (W) × 213 (H) mm
Power input	90 - 132V AC / 198 - 264V AC, 50 or 60Hz + 3Hz - auto switching.
Dimensions	500 × 500 × 482 mm (W × H × D)
Weight	29.5 kilograms (kg); 65 pounds
Power Management	Meets International Energy Star requirements: Suspend mode is <5W; Active-off mode is <5W
Certifications	UL, CSA, DHHS, FCC Class B, MPR-II, CE Mark, TCO-92 compliant, TCO-95 compliant, PC'99

5.2.2 Camera

The digital camera available for the testing of the pre-compensation was the SONY Digital Mavica MVC-FD65 digital still camera. It has a maximum CCD resolution of 2.1 megapixels, at full RGB color. Additionally, the LCD display on the rear face of the camera has a resolution of 0.1 megapixels. The size of the LCD display is approximately 5.0cm x 3.75cm (W x H). Additionally, the camera is capable of displaying, real-time, images being captured. This feature allows for instant delivery of information from the

digital monitor, through the camera, to the subject. This is a necessary feature because the images will constantly be changing on the monitor as the test proceeds.

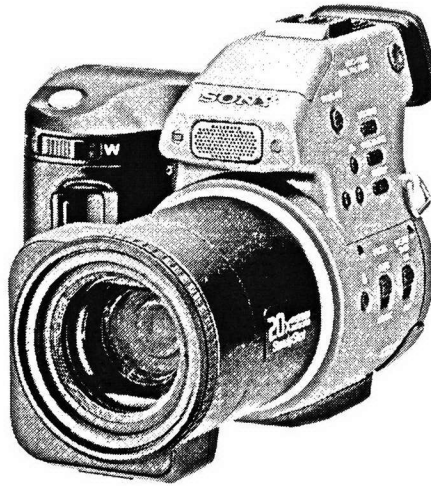


Figure 5-2: Sony Mavica MVC-FD95 Digital Still Camera

Another feature that is essential is the zoom. The camera has a 10-times zoom, allowing the placement of the monitor at any distance, so long as it is within the range of zoom of the camera.

Table 5-2: SONY Mavica Specifications

Image Device	1/2.7 type color CCD
Lens	10x zoom lens
	f=6.0 - 60.0mm (1/4 - 2 3/8 inches) (39 - 390mm)(1 9/16 - 15 3/8 in) when converted into a 35mm still camera)
	F=2.8
LCD Screen	Used LCD panel TFT (Thin Film Transistor active matrix) drive
	Total number of dots: 180000 (800x225) dots

The zoom level can be adjusted so that the viewing area of the monitor occupies the entire viewing area of the LCD. This allows for the proportions of the letters, and the

angles subtended by the letters to be controlled. The specifications for the camera can be found in table 5-2.

5.2.3 Lens

The lens used to introduce the aberration into the visual system of the subjects was an optical grade, hard coated, single vision lens made of CR-39 with a diameter of 70mm (see Figure 5-3). This lens was chosen because it introduced the strongest second order, spherical distortion, amongst lenses of this type available from Rainbow World, Inc., a local optical supplies vendor. A simple spherical defocus was chosen because of its simplicity, but also for its impact in distorting the images when placed in front of the camera. The wavefront error for this lens is shown in Figure 5-4.

Figure 5-3: Optical grade lens with Sphere = -6.0

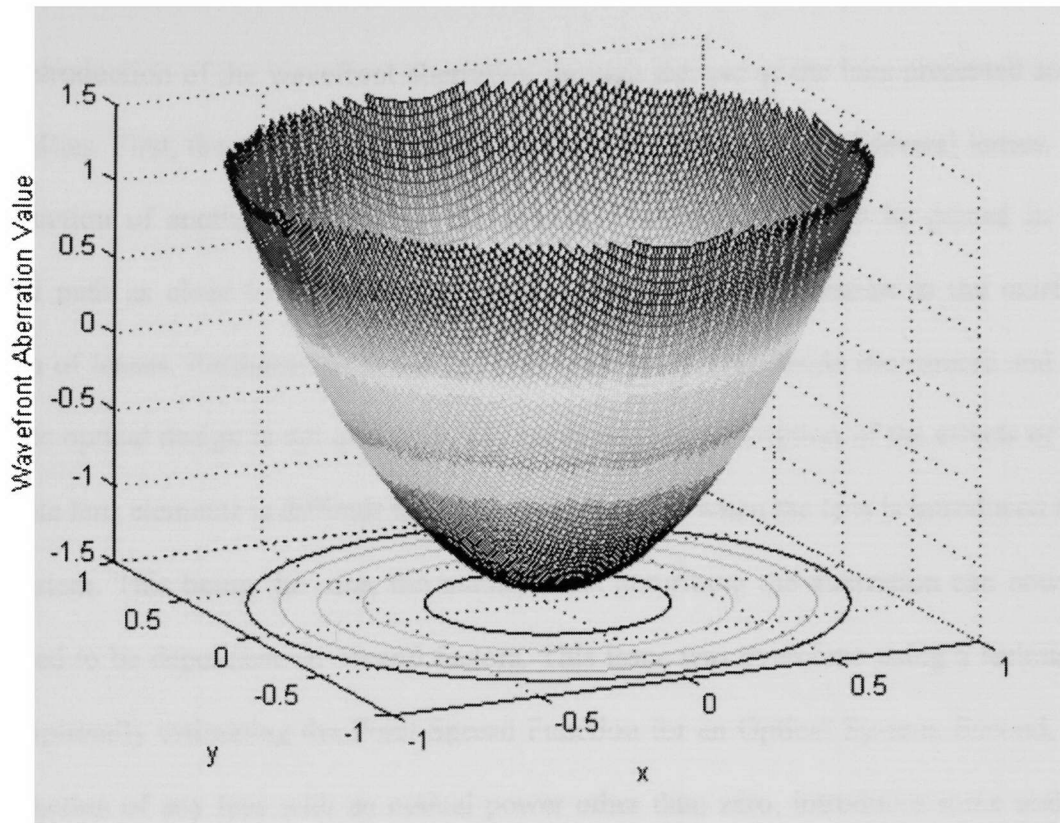


Figure 5-4: Wavefront aberration for the -6.0 D lens used.

5.2.4 Personal Computer

The Personal Computer chosen to be the platform for computation and delivery of the images was a Gateway PC, with an Intel 1.0 GHz Pentium processor and 256Mb of system memory. The operating system of the PC is Windows© 2000. The main tool used to implement the necessary image processing is MATLAB©. Once the images were pre-compensated and stored on the hard disk, visual presentation was achieved using Adobe Photoshop©.

5.3 Introduction of Wavefront Aberration

The introduction of the wavefront aberration through the use of the lens presented some difficulties. First, the camera itself has an optical system composed of several lenses. An introduction of another lens outside the camera, even though it will be placed in the optical path as close to the outer lens as possible, adds an aberration to the existing system of lenses. Furthermore, since the lenses are physically inside the camera and the specific optical design is not available, any mathematical description of the effects of the multiple lens elements is difficult to obtain, even more so when the lens is introduced into the system. This being the case, the mathematics describing the aberration can now be assumed to be dependent on several factors. This issue was overcome using a technique for empirically estimating the Point Spread Function for an Optical System. Second, the introduction of any lens with an optical power other than zero, introduces some scaling into the image. In the case of a -6.0 D lens, the scaling is significant.

5.3.1 Scaling

If all of the parameters of the entire optical system are known, using the equations from chapter two, the scaling can be found. Thus, it can be compensated for by moving the camera along the visual axis a certain distance (given by the equations in chapter two) in essence undoing the effect of scaling introduced by the lens. But, the scaling of the system with the introduction of the lens is difficult to calculate, given the multiple lens elements of the zoom on the camera, all of which are unknown and internal to the camera. This difficulty can be overcome by moving the camera closer to the digital monitor, thereby undoing the magnification effect, until the display area of the monitor

occupied the entire contents of the LCD display, circumnavigating the need for any rigorous calculations with unknown parameters. The resulting images displayed to the subject will subtend the same visual angle, without the effect of scaling.

5.3.2 Determining the true Wavefront Aberration

Due to the Sony Mavica's multiple lens elements creating the zoom feature, it was decided that the PSF was to be estimated empirically. The PSF, or impulse response for any linear, shift invariant system, can be determined if both the input and the output to the system are known. In an optical system, the easiest way to determine the PSF is by creating a point source of monochromatic light, and recording the output, in the form of an image (either digital or analog). In reality, a point source of light is seldom available or is very difficult to create. In the case of this project, the ability to take images through the digital camera is available. Furthermore, the optical aberration can be introduced or removed at will, which allows for images to be taken with and without the aberration. Thus, a four-step approach can be taken in determining the point spread function.

1. Obtain an image of an approximate point source of light.
2. Adjust the position of the camera to overcome the negative scaling introduced by the lens, and obtain an image through the aberration with the lens present.
3. Use the Minimum Mean Square Error filter approach (see Chapter 4) to deconvolve the input image from the output image. The result is the PSF due to the introduction of the lens.
4. Derive the analytical model for the PSF that matches the model given by the empirical methods using the equations from Chapter 2.

This procedure was carried out, and the PSF was determined for a lens with a refractive power of -6.0 D (Spherical -6.0). The point source of light was created using a sodium-mercury lamp which gives near monochromatic light in the range of about 550 to 600 nm [19].

An artificial aperture, 1/32 of an inch in size, was introduced using sheet metal to cover the entire contents of the lamp, and only allow a small point of light to be projected. In order to limit the intensity of light to a recordable level and avoid saturation of the CCD, several layers of clouded plastic were placed over the aperture. Figures 5-5 through 5-7 show the image of the point source as taken by SONY Mavica, the image taken after the introduction of the aberration, and the resulting deconvolved PFS, respectively.

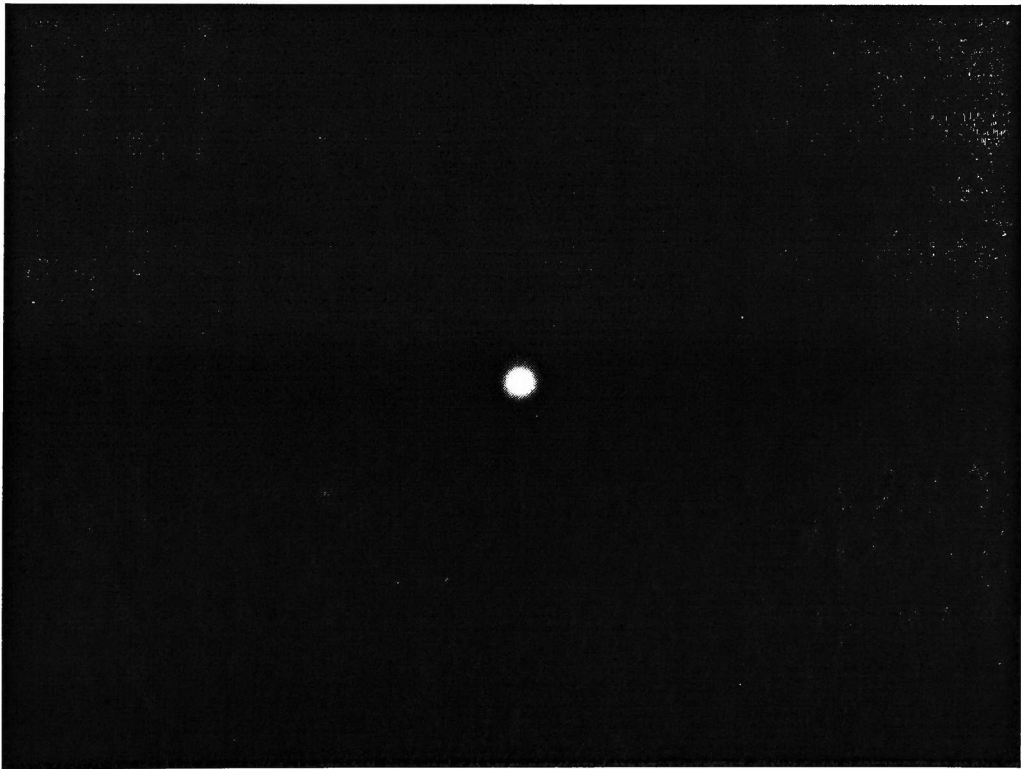


Figure 5-5: Image of approximated point source

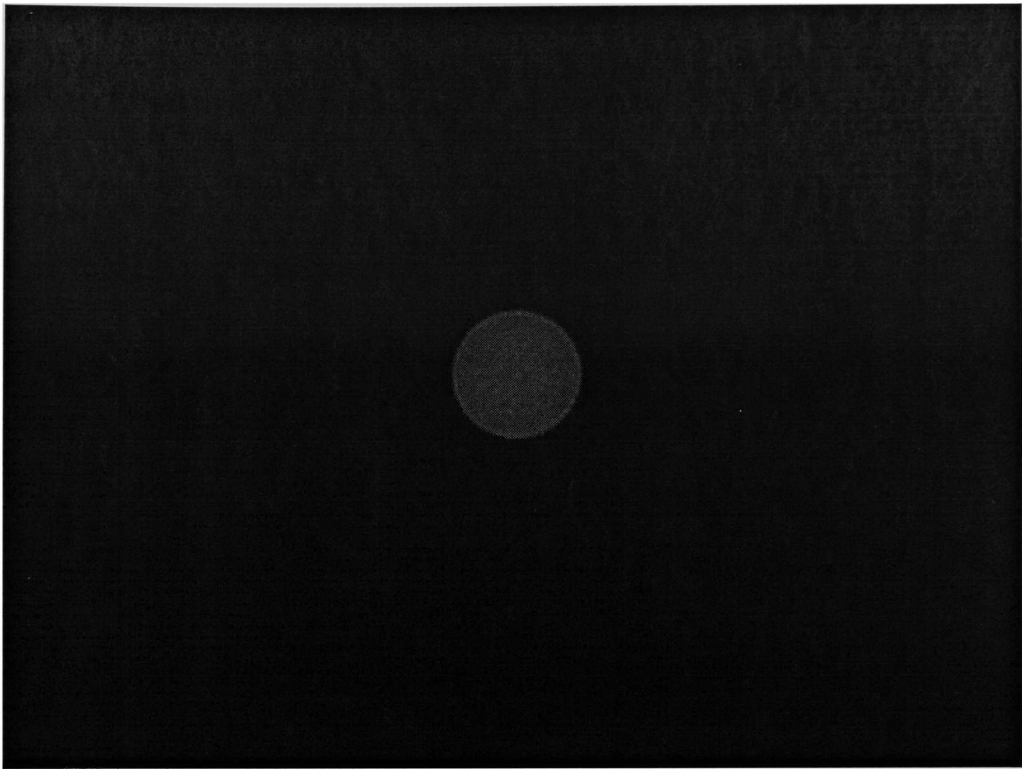


Figure 5-6: Resulting, blurred image of point source due to the introduction of the -6.0 lens

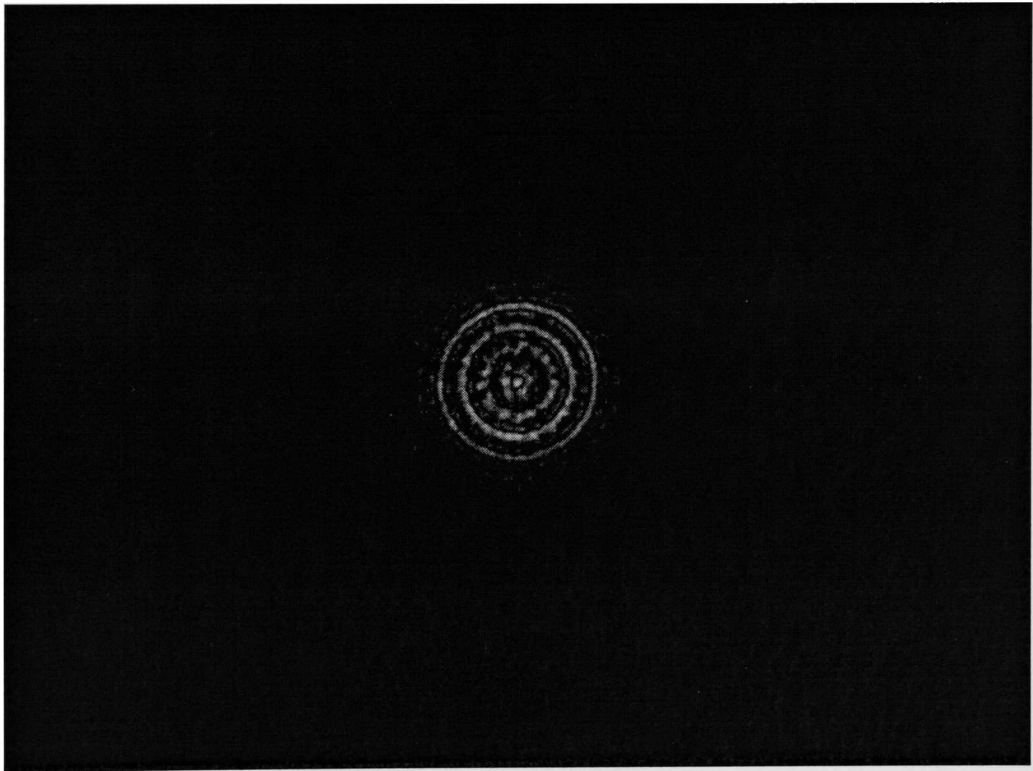


Figure 5-7: Resulting PSF from deconvolving figure 5-4 from 5-5 (Enhanced for Display)

Figures 5-8 through 5-10 show a three dimensional mesh of the entire process.

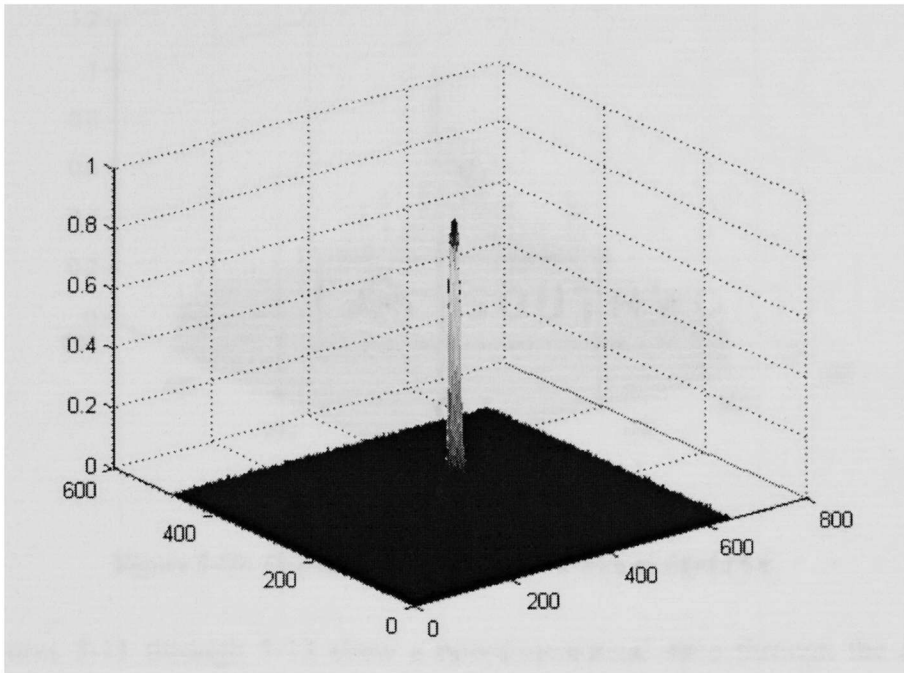


Figure 5-8: Two-dimensional representation of figure 5-4

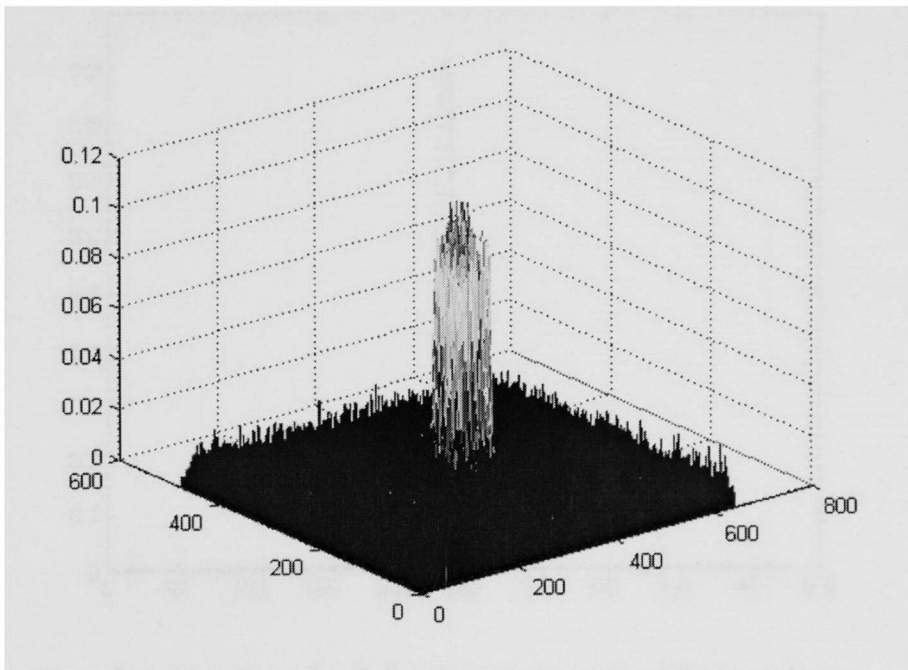


Figure 5-9: Two-dimensional representation of figure 5-5

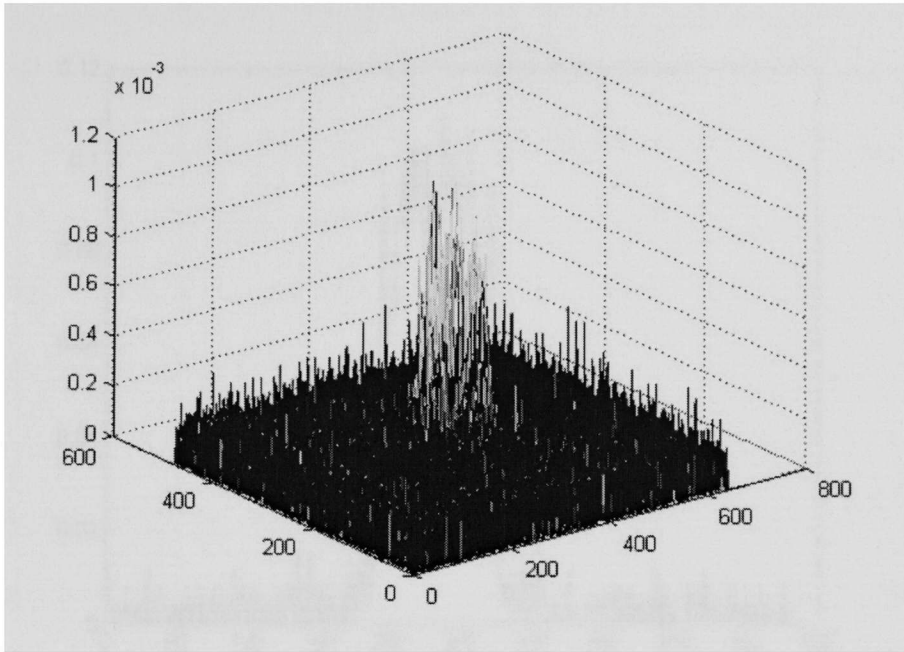


Figure 5-10: Two-dimensional representation of figure 5-6

Figures 5-11 through 5-13 show a one-dimensional slice through the center of each image in the process.

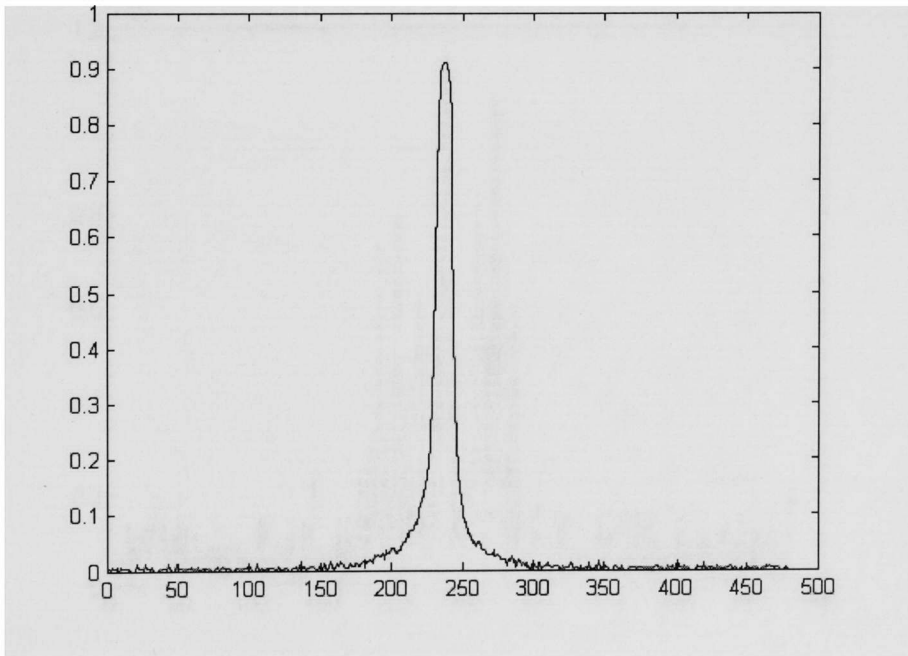


Figure 5-11: One-dimensional slice through the center of the Input Image.

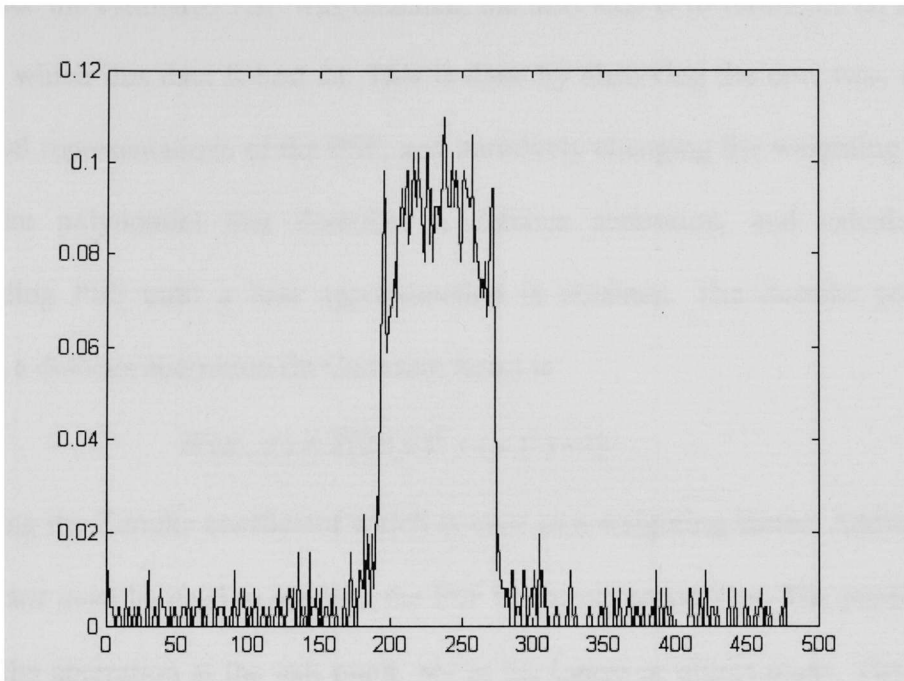


Figure 5-12: One-dimensional slice through the center of the Output Image.

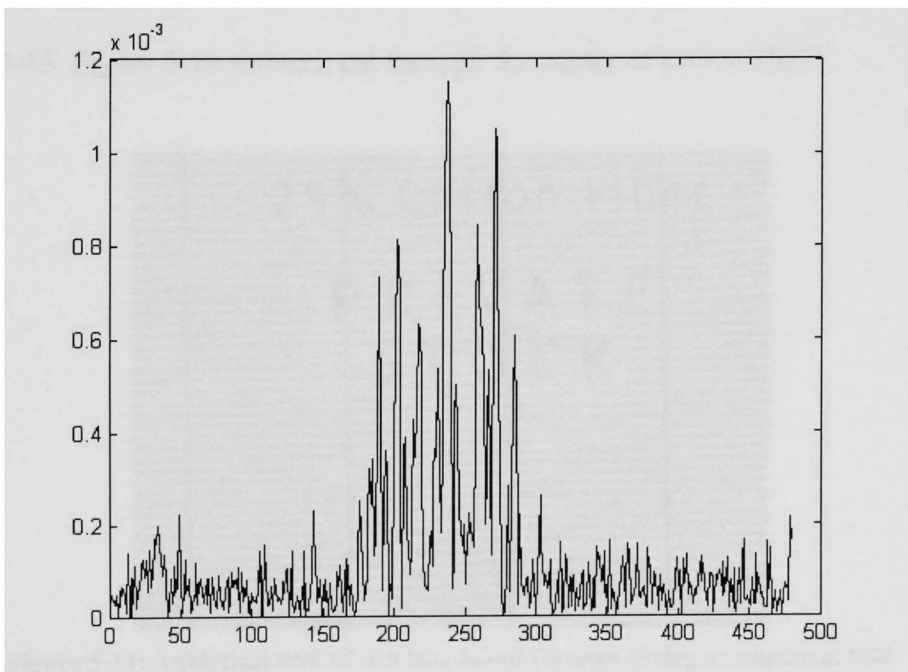


Figure 5-13: One-dimensional slice through the center of the PSF Image.

Once the estimated PSF was obtained, the next step is to formulate an analytical model for which this data is best fit. This is done by observing the one, two, and three dimensional representations of the PSF, and iteratively changing the weighting factor of the Zernike polynomial that describes a defocus aberration, and calculating the corresponding PSF until a near approximation is obtained. The Zernike polynomial describing a defocus aberration (in Cartesian form) is

$$W(x', y') = Z[2((x')^2 + (y')^2) - 1] \quad (5.1)$$

with Z being the Zernike coefficient which is used as a weighting factor. Additionally, a scaling factor must be used to produce the PSF in correct proportion. The pupil function describes the aberration at the exit pupil, not in the image or object plane. The program used to determine the PSF can be found in the Appendix. Through successive iterations, the value of Z was found to be 1.4, and the scaling factor was found to be 4. The resulting PSF used to apply the pre-compensation is shown in two and three dimensions in figures 5-14 and 5-15. Figure 5-16 shows a cut through the center of such a PSF.

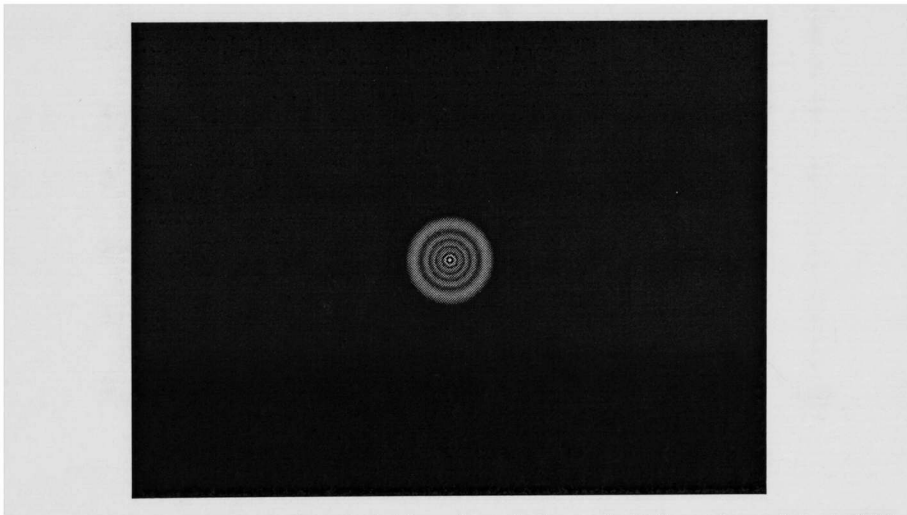


Figure 5-14: Analytical PSF of -6.0 lens found through fitting of empirical PSF

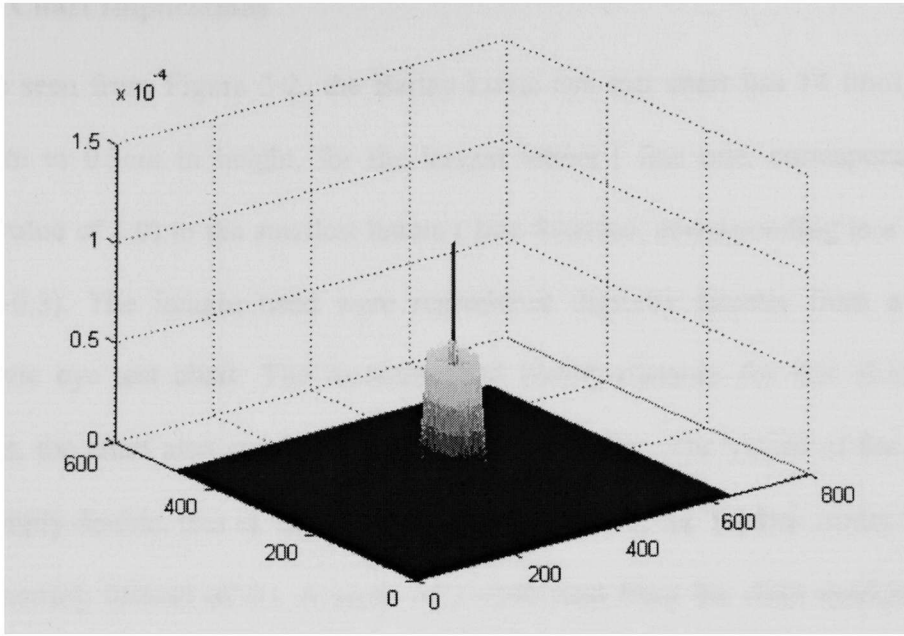


Figure 5-15: Two-dimensional mesh of figure 5-13

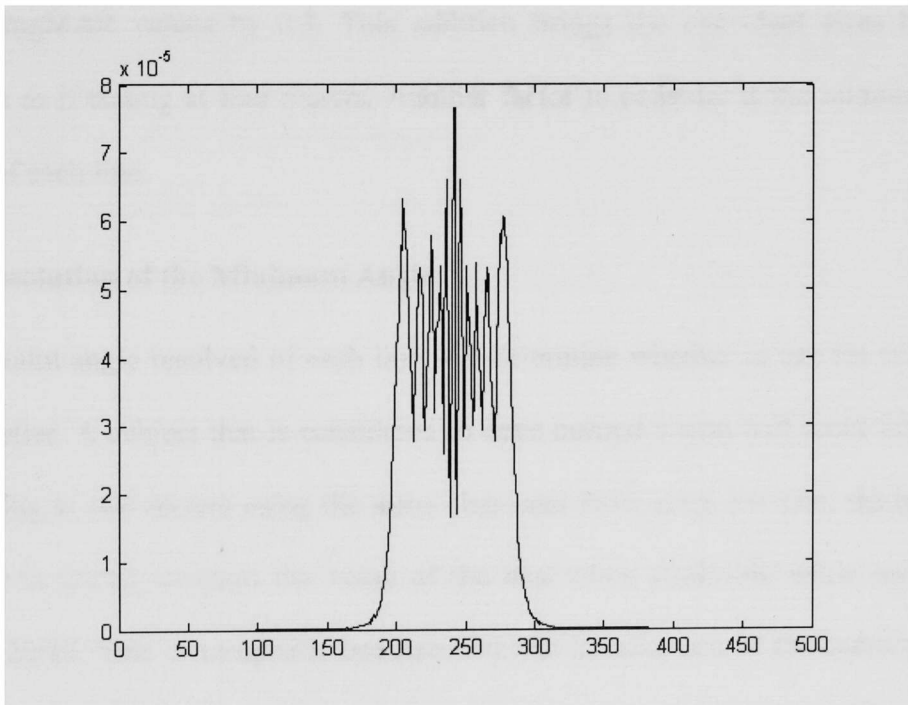


Figure 5-16: One-dimensional slice of Analytical PSF

5.4 Eye Chart Implications

As can be seen from Figure 3-2, the Bailey-Lovie eye test chart has 14 lines, ranging from 5.8cm to 0.3cm in height, for the largest letters (line one, corresponding to a logMAR value of 1.0) to the smallest letters (line fourteen, corresponding to a logMAR value of -0.3). The images used were reproduced digitally directly from a life-size Bailey-Lovie eye test chart. The recommended testing distance for this chart is four meters, but, the chart also can be used at a distance of 2m. The values of the resulting acuities simply double, that is, the value of the numerator of the Snellen acuity would be 10 (3 in metric), instead of 20. A score of 20/200 read from the chart markings while testing at 2 meters, would in reality be 10/200, or equivalently 20/400. Instead of adjusting the Snellen number, a more efficient way of adjustment is to bias all of the resulting logMAR values by 0.3. This addition brings the eye chart sizes back into proportion as if testing at four meters. Another factor to consider is the minimum angle resolved of each line.

5.4.1 Resolution of the Minimum Angle

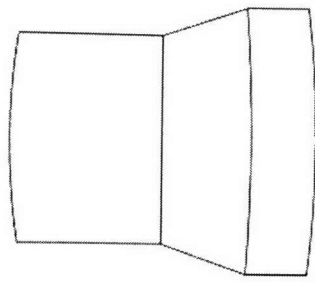
The minimum angle resolved of each line will determine whether or not the subject can read the letter. A subject that is considered to have normal vision will score 20/20. But, while testing at two meters using the same chart and letter sizes per line, the best score recordable is 20/20, whereas the value of the best score attainable while testing at 4 meters is 20/10. This is acceptable because with the introduction of the camera into the visual process, there is a decimation in the visual resolution of the monitor. The sampling rate of the LCD is approximately 16000 pixels per meter. According to the Nyquist

criteria, the maximum spatial frequency allowed without aliasing is 9800 pixels per meter. This sampling frequency corresponds to a minimum spacing between black and white transitions of 0.125 mm on the LCD. The scaling ratio between the size of the monitor and the size of the LCD display is approximately 40.6 cm:5.0 cm, or 8.12:1. This corresponds to an $8.12 \times 0.125 \text{ mm} = 1.015 \text{ mm}$ minimum separation between black and white transitions in the eye test chart. Thus, lines thirteen and fourteen will not be able to be read accurately by any subject because the minimum separation between black and white in any letter is less than one millimeter. Therefore, the most that is expected from any subject participating in the experiment would be the ability to read the letters up to line twelve.

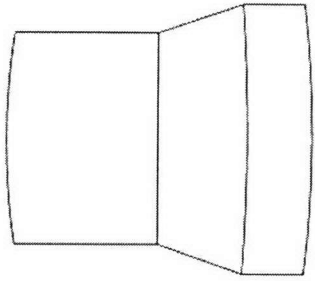
5.5 Testing Procedure

In order to expedite the testing, all of the images of the each line of the eye were first created and pre-compensated. The testing procedure is as follows:

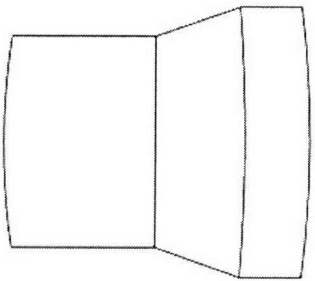
1. Mount the digital camera onto a tripod, approximately 2 meters from the monitor.
The testing distance assumed for the eye test chart is $\frac{1}{2}$ the maximum distance of 4 meters.
2. With the camera turned on, position the camera so that the visual axis intersects the center of the monitor screen.
3. Using the zoom button, zoom the camera in on the monitor until the viewable area of the monitor occupies the entire display LCD on the camera.



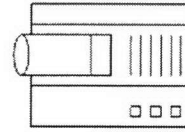
PC Monitor



PC Monitor



PC Monitor

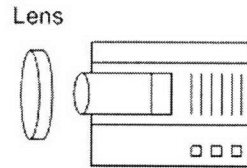


Digital Camera



Subject's Eye

(a)



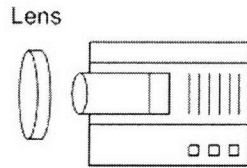
Lens

Digital Camera



Subject's Eye

(b)



Lens

Digital Camera



Subject's Eye

(c)

Figure 5-17: Experimental Setup (a) Top - Standard Eye Test, No Aberration Present (b) Middle – Blurred Eye Test, Aberration Present (c) Bottom – Pre-compensated Eye Test, Aberration Present, Correct Wavefront.

4. Explain to the subject the entire experiment, including the testing procedure, the risks involved, and the instructions to be given during the exam. Additionally, the subject is to read and sign the “Consent to Participate in a Research Study” form. (A copy can be found in the Appendix, along with the IRB approval)

5. Place the subject behind the digital camera, approximately 6 inches from the LCD panel located on the back end of the digital camera. An adjustable chair can be used to match the eye level of each subject with the height of the LCD panel.
6. Using Adobe Photoshop, open all of the images of the digital eye test chart, with and without pre-compensation.
7. There will be three runs of the following procedure for each eye, both the right and left, independently, totaling six exams per subject:
 - a. Display, starting from line one, each line of the eye test chart.
 - b. For each line, have the subject identify the letters to the best of his/her ability.
 - c. Use the scoring sheet found in the Appendix to mark the subject's answer for each letter. Circle correctly identified letters and cross out letters not identified.
8. For the first of the three runs, the subject will identify the letters without the introduction of the aberration, displaying the normal, un-compensated, eye test chart lines.
9. For the second of the runs, place the -6.0 lens in front of the camera, as close to the lens of the camera as possible. Move the camera approximately 88cm closer to the monitor along the visual axis. Use the same, normal un-compensated images for the test.
10. Now, follow the same procedure as in step 9, but use the pre-compensated eye test chart lines.

11. Obtain a single visual acuity score from each scoring sheet using the procedure outlined in chapter 3 for the assessment of E, the visual efficiency value.

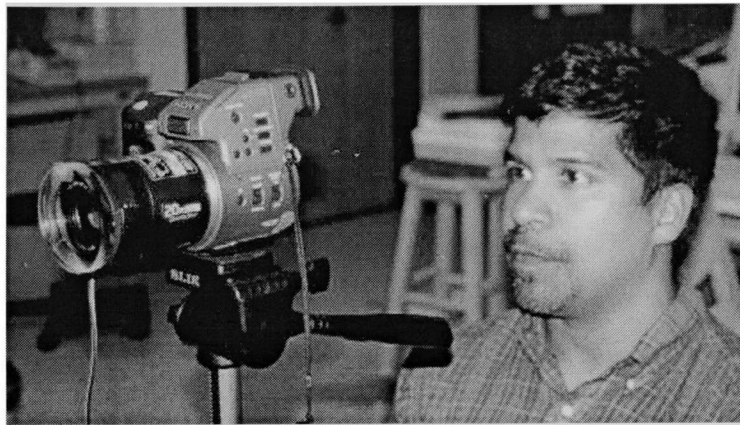


Figure 5-18: Image of Subject participating in the Study - After the introduction of the Lens

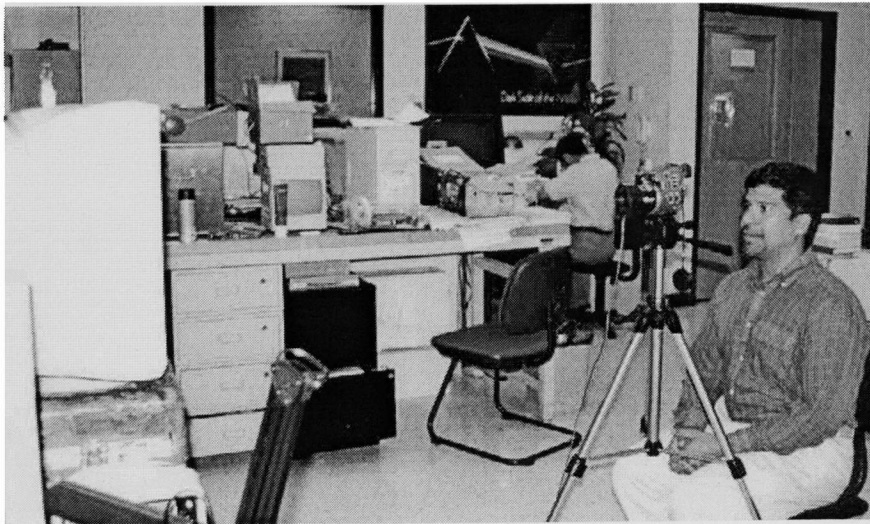


Figure 5-19: Image of Subject - Before the Introduction of the Lens



Figure 5-20: Image of Subject - Also, Before the Introduction of the Lens

6 RESULTS AND DISCUSSION

6.1 Simulated Experiment for -6.00 Diopter Sphere Lens

The procedure outlined in chapter 5 for obtaining the PSF of the -6.0 D lens, as well as for generating the pre-compensated image, was accomplished using MATLAB. Figure 6-1 shows the analytical PSF obtained using said procedure, scaled and resized. Additionally, this image has been cropped and padded to match the image size of the eye test chart lines, shown in Figure 6-2. This is necessary due to the fact that both the image and the PSF need to be of the same size in order to implement the minimum mean square error deconvolution described in chapter 4. Another key factor to this process is that the eye test chart lines, when displayed on-screen, are equivalent in size to an actual eye test chart. This is important because it ensures that the test can be properly administered.

Figure 6-4 shows the results of the pre-compensation. This is the image that compensates for the aberration introduced by the -6.0 D lens. This image was produced using equation 4.8 with a K value of 0.0005.

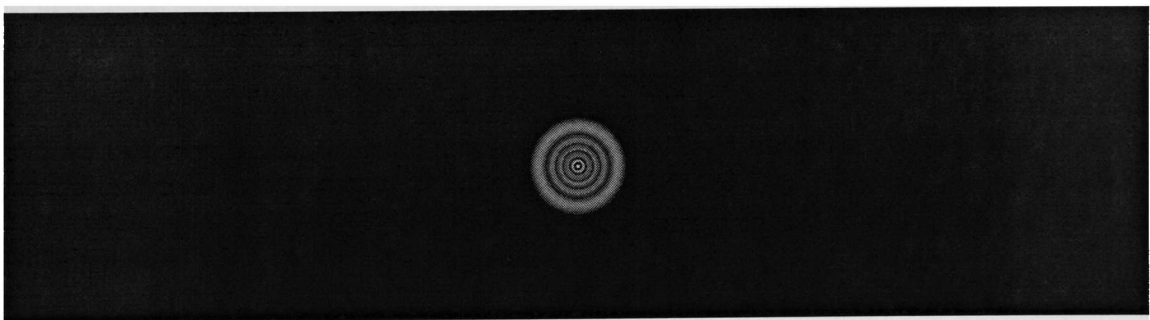


Figure 6-1: Analytical PSF generated for testing



Figure 6-2: Digital Image of Eye Test Chart Line 1

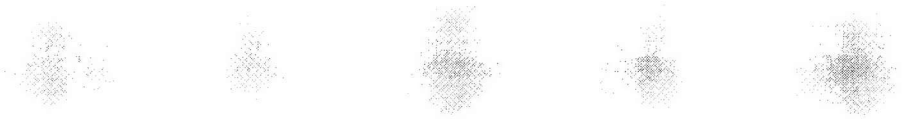


Figure 6-3: Simulation of Digital Image of Eye Test Chart Line 1 viewed through the -6.0 D lens

It is important to note that the direct result of the pre-compensation is not a displayable image, having values that range well above 255 and below zero. In order to reduce this swing, the eye test chart images are normalized to 255. The pre-compensation is then done, and the resulting pre-compensated image is rescaled by a factor of 80. This factor was chosen on an iterative basis, by scaling and displaying the resulting pre-compensated image as an 8-bit grayscale image with every iteration until a suitable visual image was obtained when viewed through the -6.0 D lens. This display process truncates the image, making any values that are less than 0 equal to 0, and values larger than 255 equal to 255. Once the entire procedure to produce the pre-compensated images is complete, the images are saved on the computer in an 8-bit format, using the same scaling factor and truncation. A three dimensional mesh of the final, scaled and truncated,

display image is shown in Figure 6-7. Once this image is viewed through the lens, the pre-compensation is cancelled, resulting in a sharper image. This cancellation process was simulated using the same PSF and convolving it with the pre-compensated image. The result is shown in Figure 6-5. As can be seen in Figure 6-5, once the pre-compensated image is viewed through the -6.0 D, it is brought back into focus. There is, however, a loss of contrast due to the post processing done on the pre-compensated image, namely the scaling and truncation.

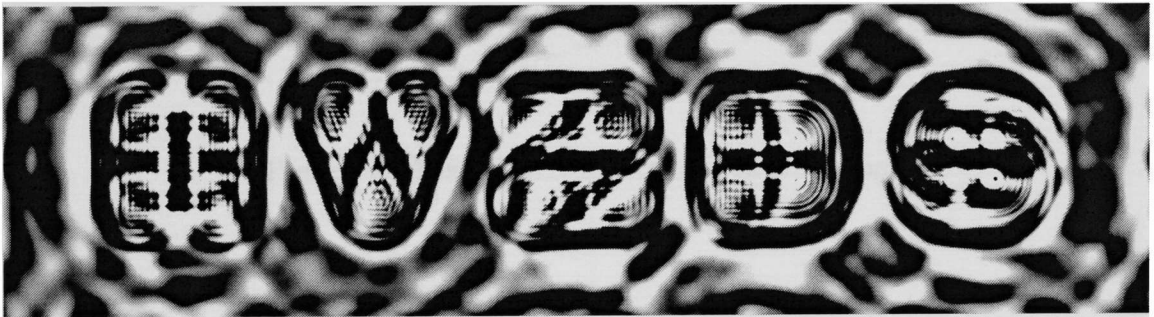


Figure 6-4: Pre-compensated Eye Test Chart Line 1

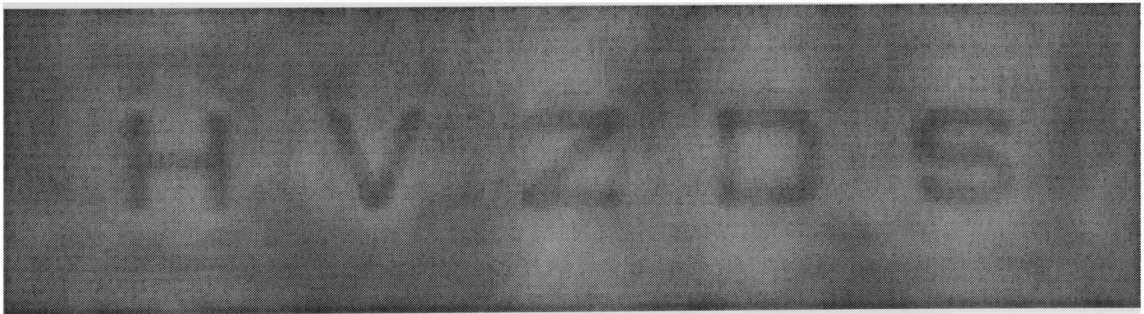


Figure 6-5: Simulated Retinal Image, that is, what the viewer will see when looking at Figure 6-3 through the -6.0 D lens

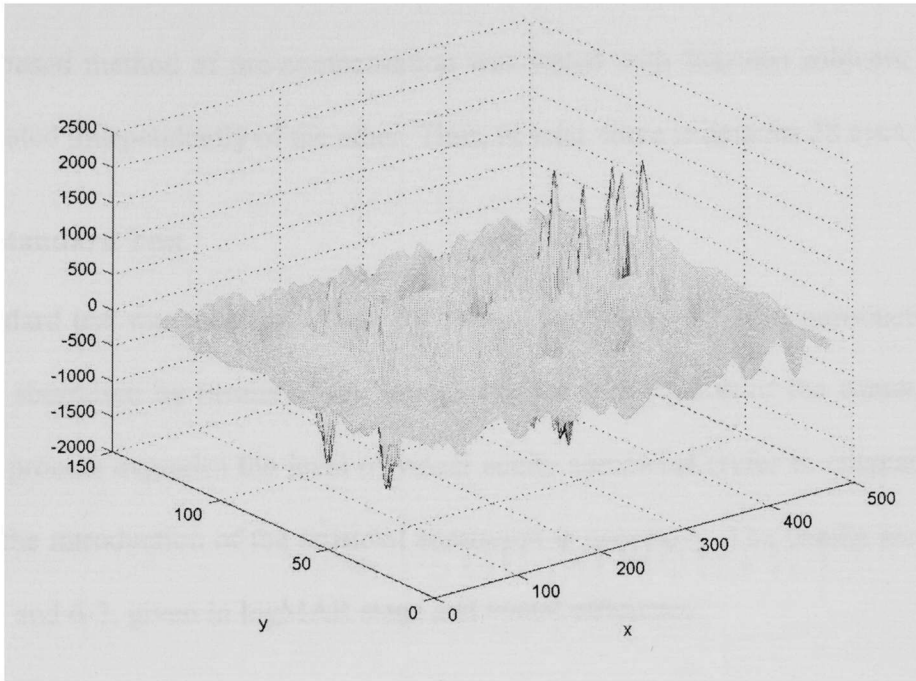


Figure 6-6: Mesh of Figure 6-4 without post processing.

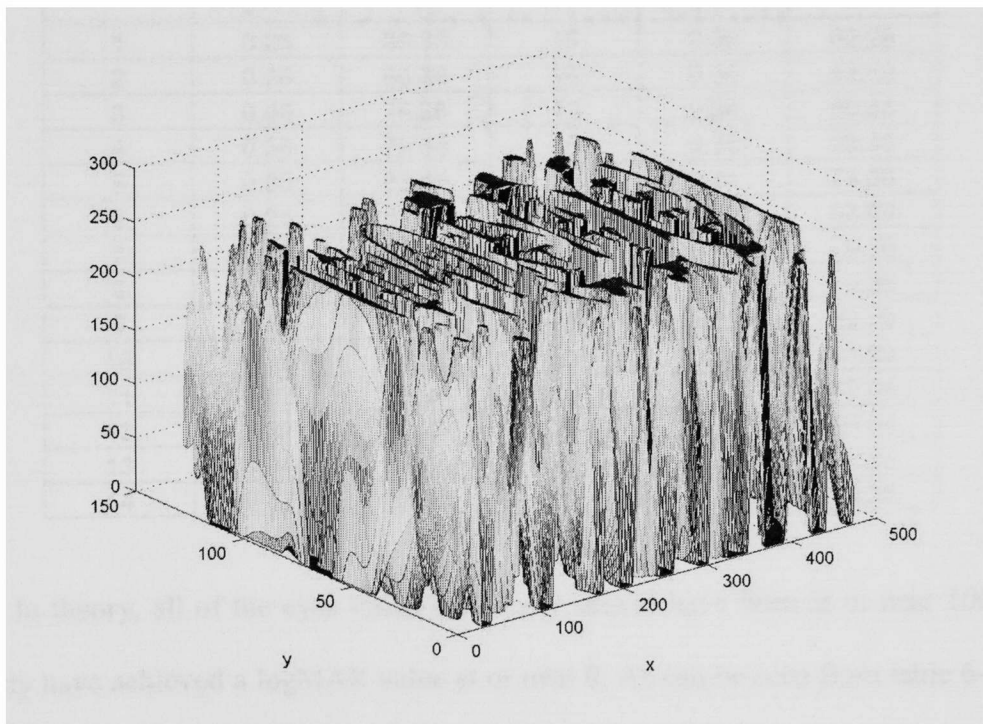


Figure 6-7: Figure 6-4 after post processing.

6.2 Results

The proposed method of pre-compensation was tested with fourteen subjects, each eye being treated independently of the other. Thus, in total, there is data for 28 eyes.

6.2.1 Standard Test

The standard test was taken as a base for comparing the results after introduction of the artificial aberration by means of the lens. Since the introduction of the camera into the imaging process degrades the level of visual acuity somewhat (refer to chapter 5), a test without the introduction of the artificial aberration is necessary. The results are shown in table 6-1 and 6-2, given in logMAR steps and visual efficiency.

Table 6-1: Results of the Standard Test for 28 eyes

Eye ID	Visual Acuity (logMAR)	Visual Efficiency (%)	Eye ID	Visual Acuity (logMAR)	Visual Efficiency (%)
1	0.26	86.36	15	0.32	82.29
2	0.26	86.36	16	0.30	83.69
3	0.40	76.30	17	0.34	80.86
4	0.36	79.38	18	0.36	79.38
5	0.30	83.69	19	0.44	73.06
6	0.24	87.63	20	0.30	83.69
7	0.34	80.86	21	0.40	76.30
8	0.36	79.38	22	0.36	79.38
9	0.36	79.38	23	0.32	82.29
10	0.36	79.38	24	0.30	83.69
11	0.32	82.29	25	0.28	85.04
12	0.32	82.29	26	0.28	85.04
13	0.34	80.86	27	0.38	77.86
14	0.32	82.29	28	0.36	79.38

In theory, all of the eyes visual efficiency should have been at or near 100%, or similarly have achieved a logMAR value at or near 0. As can be seen from table 6-1, this is not the case. The deviation from the expected value arises from the introduction of the

camera into the imaging process (see chapter 5). Clearly, the results were as predicted in chapter 5. Most subjects read up to line eleven, with some subjects reading letters on the twelfth line, as is evident by table 6-2. The mean value of visual acuity in units of logMAR was found to be 0.33, which corresponds, after adjustment, to an efficiency better than the required to read up to line 10, but less than the required to read up to line 11. The standard deviation of the logMAR values, 0.05, indicates that the majority of the subjects scored very close to 0.33.

Although there is a deviation from the ideal, the visual efficiency of the subjects did not suffer a great deal, the average visual efficiency being 81.37%. This is well above the maximum efficiencies achieved after the introduction of the artificial aberration. The efficiencies were found not to exceed 81%, as will be shown in the following sections.

Table 6-2: Mean and Standard Deviation for Standard Test

	Visual Acuity (logMAR)	Visual Efficiency (%)
Mean	0.33	81.37
Standard Deviation	0.05	3.32

6.2.2 Blurred Test

With the introduction of the -6.0 diopter lens in front of the camera, the image displayed is extremely blurred. Evidently, all of the lines from the eye test chart will be severely distorted. The impact of the distortion on the readability of the letters increases as the size of the letters decreases from line to line. Table 6-3 shows the results for the eye test chart when subjects viewed it through the aberration. Although this aberration is only of second order, the blur introduced causes many letters to be distorted beyond recognition.

The average visual acuity score for the blurred test is 1.37 with a standard deviation of 0.5 logMAR units. However, the significant decrease in acuity introduced by the blur is more evident when comparing the visual efficiency. The average visual efficiency is only 1.92% with a standard deviation of 1.41%. The standard deviation is relatively large compared to the mean. This is primarily due to the eyes with ID's 27 and 28, scoring a visual efficiency of 6.14% and 7.02%. It is interesting to note that these two eyes belong to the same person. Apparently, when compared to the other subjects tested, this subject (with either eye) has a more refined ability to identify patterns through a visual aberration.

Table 6-3: Results of the Blurred Test for 28 eyes

Eye ID	Visual Acuity (logMAR)	Visual Efficiency (%)	Eye ID	Visual Acuity (logMAR)	Visual Efficiency (%)
1	1.34	2.39	15	1.40	1.34
2	1.38	1.64	16	1.38	1.64
3	1.40	1.34	17	1.40	1.34
4	1.40	1.34	18	1.38	1.64
5	1.40	1.34	19	1.40	1.34
6	1.40	1.34	20	1.36	1.98
7	1.40	1.34	21	1.40	1.34
8	1.40	1.34	22	1.40	1.34
9	1.34	2.39	23	1.40	1.34
10	1.36	1.98	24	1.40	1.34
11	1.38	1.64	25	1.40	1.34
12	1.40	1.34	26	1.40	1.34
13	1.36	1.98	27	1.22	6.14
14	1.36	1.98	28	1.20	7.02

This ability is not due to the physical optics behind the testing, evident by the variability of the results. There are several aspects to human perception, including vision, that are somewhat dependent on higher cognitive reasoning. Pattern recognition is an example of high cognitive task. The superior ability for pattern recognition that this

subject exhibited, despite the distortion, may be due to several factors, all of which are beyond the scope of this thesis. On the average however, the visual efficiency was reduced from approximately 82% to 2%, an extreme reduction in visual efficiency. Thus, this aberration can be considered to be a severe visual impairment, even though it is only of second order.

Table 6-4: Mean and Standard Deviation for Blurred Test

	Visual Acuity (logMAR)	Visual Efficiency (%)
Mean	1.37	1.92
Standard Deviation	0.05	1.41

6.2.3 Pre-compensated Test

Table 6-5: Results of the Pre-compensated Test for 28 eyes

Eye ID	Visual Acuity (logMAR)	Visual Efficiency (%)	Eye ID	Visual Acuity (logMAR)	Visual Efficiency (%)
1	0.64	54.77	15	0.76	42.72
2	0.66	52.79	16	0.72	46.77
3	0.58	60.57	17	0.74	44.74
4	0.64	54.77	18	0.70	48.78
5	0.64	54.77	19	0.66	52.79
6	0.64	54.77	20	0.70	48.78
7	0.70	48.78	21	0.74	44.74
8	0.72	46.77	22	0.64	54.77
9	0.64	54.77	23	0.64	54.77
10	0.68	50.79	24	0.66	52.79
11	0.66	52.79	25	0.68	50.79
12	0.70	48.78	26	0.70	48.78
13	0.62	56.73	27	0.64	54.77
14	0.62	56.73	28	0.66	52.79

The results for the pre-compensated test indicate that the improvement in visual acuity and efficiency is significant. The results are shown in tables 6-5 and 6-6. The average visual acuity dropped from the value of 1.37 (logMAR units), to a value of 0.67.

Similarly, the visual efficiency increased more than 20 fold, from a very low value of 1.92%, to a much higher value of 51.69%. The standard deviations for both the visual acuity and visual efficiency indicate that all of the subject's performances were very close to the mean. Table 6-6 shows the standard deviations of the acuity and efficiency.

Although the results show promise, they evidently do not show complete restoration of visual acuity or efficiency. This is primarily due to the trade off established in the Minimum Mean Square Error method of deconvolution discussed in chapter four. A close approximation to the real theoretical inverse is possible, but at the sacrifice of visual intelligibility.

Table 6-6: Mean and Standard Deviation for Pre-compensated Test

	Visual Acuity (logMAR)	Visual Efficiency (%)
Mean	0.67	51.69
Standard Deviation	0.04	3.95

6.3 Discussion of Results

When comparing the results obtained after the introduction of the aberration, that is, viewing through the -6.0 D lens images that were and were not pre-compensated, it is evident that the visual acuity and visual efficiency is greatly improved when the proposed approach is applied. Figure 6-1 shows the distribution of visual acuity for the standard, blurred, and pre-compensated tests. The bottom line represents the normal, standard acuity, as recorded through the digital camera. This represents the ideal situation. A lower visual acuity measurement (in logMAR) corresponds to a higher degree of visual acuity. The introduction of the aberrations pushes this distribution up towards the maximum

value of 1.4. This change corresponds to a reduction in vision from 20/40 to 20/500 measured as the Snellen distance acuity. The trace in the middle of figure 6-1 represents the partial restoration of visual acuity obtained by pre-compensating the images.

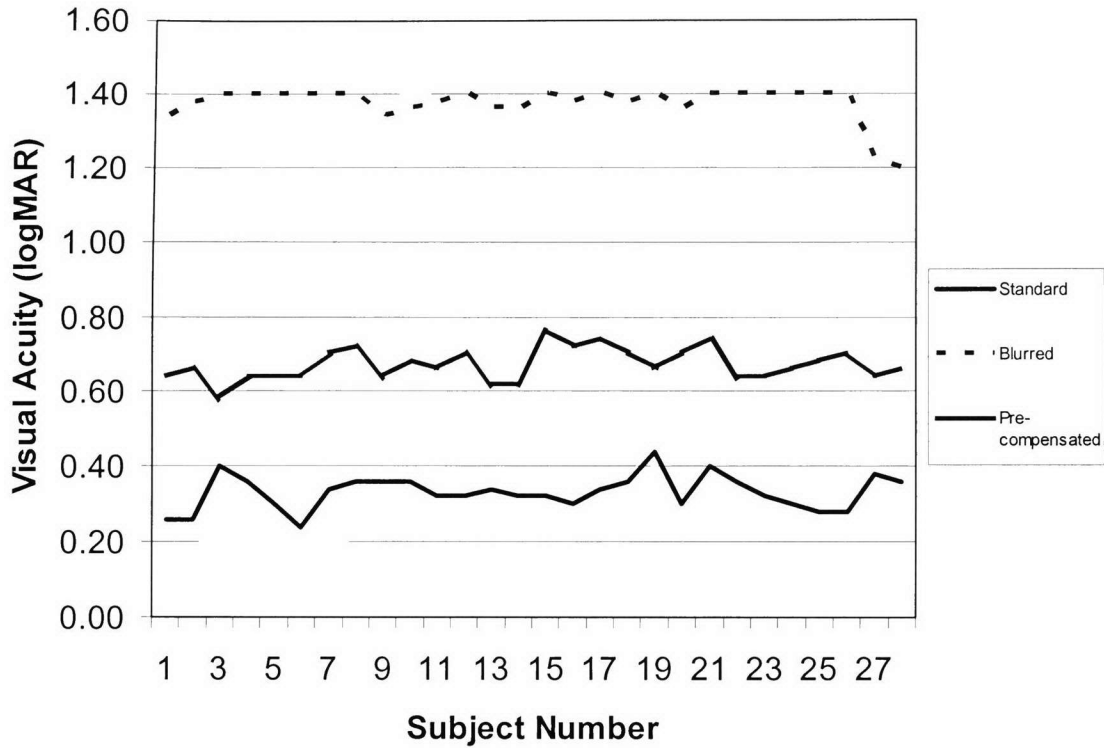


Figure 6-8: Visual Acuity vs. Eye ID

Figure 6-2 represents the change in visual efficiency across all of the eyes tested, from before the pre-compensation, to after. This is found by taking the difference between the visual efficiency for each eye before the pre-compensation is applied and the efficiency after the compensation. As can be seen in this figure, there is a consistent improvement in visual efficiency ranging from an increase by 40% to as much as 60%.

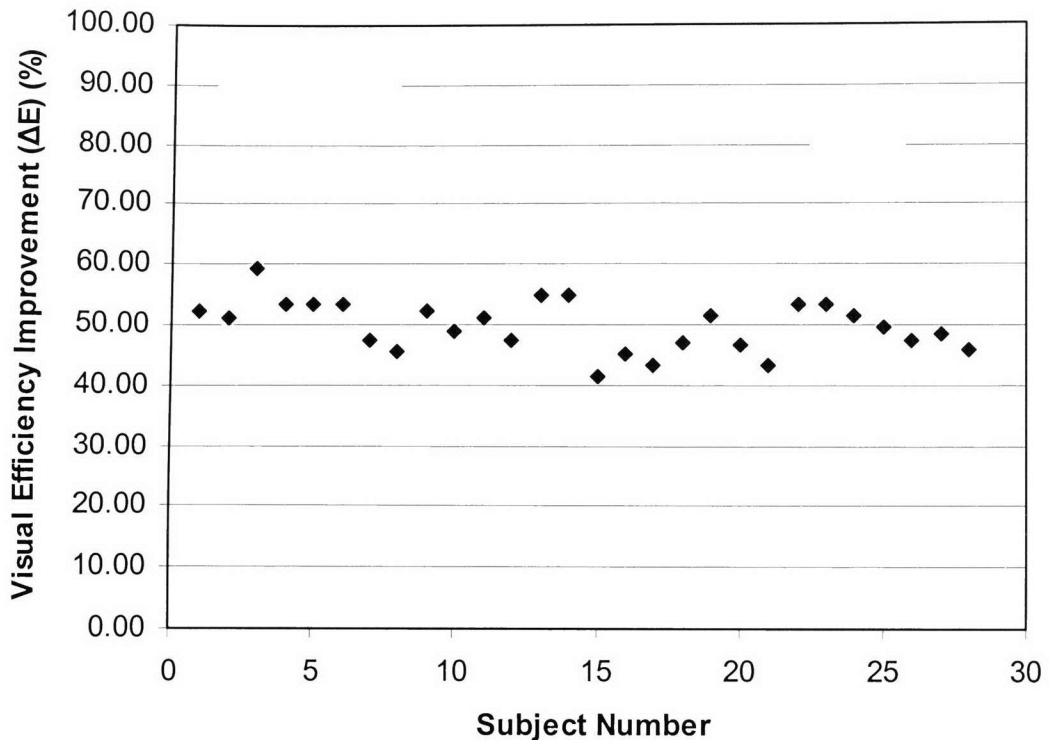


Figure 6-9: Relative Improvement of Visual Efficiency for the subjects

Figure 6-3 shows the histogram of the relative improvement of the visual efficiency. It is interesting to note the distribution is almost Gaussian. This is a common phenomenon associated with random variables appearing in nature.

Upon further analysis with respect to the improvement of computer access for the visually impaired, the results indicate that there is, in fact, an improvement in computer access. This correlation can be made under the assumption that in order to fully interface with the personal computer through vision two things must hold true.

1. The user must be able to read information displayed in the form of text.
2. The user must be able to distinguish between objects, such as icons or buttons.

The performance of a subject in an eye chart test directly relates to both of these abilities because in order to successfully read a line from the eye test chart, the subject must correctly identify the letters, which is in part reading, and in part pattern identification or object recognition.

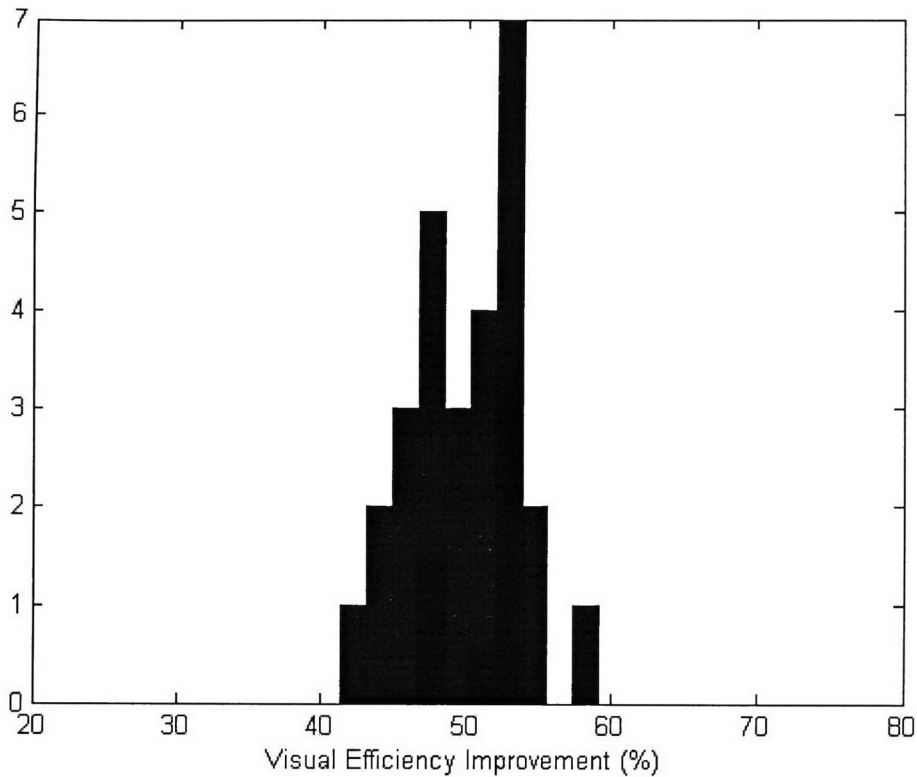


Figure 6-10: Histogram of Improvement of Visual Efficiency

7 CONCLUSION

This thesis explored the use of deconvolution as means of correcting visual aberrations in the optical system of the human eye, in an attempt to enhance the interaction of the visually impaired with computers. High order aberrations, typically considered to be of order three or higher, cannot currently be corrected through traditional means such as contact lenses or spectacles. With knowledge of the type of aberration, specifically the wavefront aberration of the particular visual impairment, the entire visual process can be simulated, providing a method of computing the retinal image for digital images displayed on a monitor. Furthermore, the inverse process, or deconvolution could be applied to the on-screen digital images before they are displayed to the user, to implement a pre-compensation for the visual limitations of the computer user. The PSF of the human eye is derived from the wavefront aberration. It is through the use of the PSF, in conjunction with a very robust method of deconvolution, that the pre-compensation of the digital images was achieved.

The method of pre-compensation was tested using a traditional way to measure the optical performance of the human visual system, the eye test chart. The eye test chart allows for an objective way of measuring visual performance with respect to a generally accepted and widely recognized standard of reporting visual performance. Specifically, the use of the Bailey-Lovie chart facilitates any statistical calculations to be made. Using these methods of reporting performance, quantitative analysis was made.

Three tests were performed on each subject. The results of the first test, using uncompensated images without the introduction of a blur, were used as a base for comparing the other two tests. The results of the second test, after the introduction of the

aberration, show the inability of most of the subjects to read past the first line of the eye test chart. This serves to indicate the severity of the distortion introduced. The results of the final test show the significant improvement achieved in visual acuity, i.e. the re-establishment of the ability to discern most of the letters of the eye test chart. This has significant implications in the ability for those subjects to interact with computers. The ability to identify and read letters is essential to this interaction. In essence, the interaction is enhanced from, marginally being able to use the computer, to being able to use the computer with little effort.

The results, however, are not, ideal. The visual efficiency is not entirely restored. But, for a person who can barely see, let alone read or interact with a personal computer, even the level of improvement achieved would be very beneficial.

Future work includes the development of a method of deconvolution that yields better visual results. Additionally, the intensity of the digital display must be significantly stronger to produce a better pre-compensated display image. This is primarily due to the fact that the blur of light spreads the energy of light over an area. This is found to be shown as the approximation to the inverse reaches the true inverse. Values of the pre-compensated image reach very large amounts, indicating a need for the ability of the monitor to display very large swings in intensity.

LIST OF REFERENCES

- [1] Bailey, I. L., and J. E. Lovie, "New design principles for visual acuity charts", *American Journal of Optometry*, 57: pp. 378-387, 1976.
- [2] Barreto, Armando B., Diner E. Elise, and Granadillo, Luis R., "Deconvolution Approaches Applied to Space-Time Radar Data", *Proceedings of SPIE: Vol. 3375, Targets and Backgrounds: Characterization and Representation IV*, pp. 256-268, 1998.
- [3] Bennet, A.G., and R.B Rabbetts, *Clinical Visual Optics, Second Edition*, Butterworths, London, 1989.
- [4] Born, M., and E. Wolf, *Principles of Optics*, 6th Edition, Pergamon Press, Oxford.
- [5] Bracewell, Ronald N., *Two-Dimensional Imaging*, Prentice-Hall Signal Processing Series, New Jersey, 1995.
- [6] Cquest.com, "Example of Advanced Keratoconus", <http://www.cquest.com/russo/Keratoconus.html>.
- [7] Center for Keratoconus, "What is Keratoconus?", http://www.kcenter.org/new/what_is_keratoconus.html.
- [8] Gateway.com, VX120 Monitor Specs, [url:http://support.gateway.com/s/MONITOR/7002139/700213915.shtml](http://support.gateway.com/s/MONITOR/7002139/700213915.shtml)
- [9] Glasser, A., & M.C.W. Campbell, "Presbyopia and the optical changes in the human crystalline lens with age", *Vision Research*, pp. 209-229, 1998.
- [10] Gonsalves, R. A., and P. Nisenson, "HST Image Processing: An Overview of Algorithms for Image Restoration, *SPIE Vol. 1567 Applications of Digital Image Processing XIV*, pp. 294-307, 1991.
- [11] Gonzales, R.C., and R.E. Wood, *Digital Image Processing, Second Edition*, Prentice Hall, New Jersey, 2002.
- [12] Goodman, J. W., *An Introduction to Fourier Optics*, McGraw-Hill, New York, 1968.
- [13] Guyton, A. C. and J. E. Hall, *Textbook of Medical Physiology*, 9th Edition, W.B. Saunders Company, Philadelphia, 1996.

- [14] Gwiazda, J., F. Thorn, J. Bauer, and R. Held, "Emmetropization and the progression of manifest refraction in children followed from infancy to puberty", *Clinical Visual Sciences*, 8: pp. 337-344, 1993.
- [15] Haykin, S., and B. Van Veen, *Signals and Systems*, John Wiley & Sons, Inc, New York, 1999.
- [16] Helmholtz, H. v., *Treatise on physiological optics, Third Edition*, Optical Society of America, 1924.
- [17] Holladay, J. T., "Proper Method for Calculating Average Visual Acuity", *Journal of Refractive Surgery, Vol. 13: pp. 388-391*, 1997.
- [18] Hopkins, H. H., *Wave theory of aberrations*. Oxford University Press, London, 1950.
- [19] Ientilucci, E., "Measurement of the Spectral Distribution of Gas Discharge, Fluorescent and Incandescent Sources", 2000.
- [20] Kinsburg, A. P. and W. R. Hendee, "Quantification of Visual Capability", *Chapter 3 in The perception of visual information, pp. 55-72*, Springer –Verlag, 1993.
- [21] Liang, J., B. Grimm, S. Goelz, and J. Bille, "Objective Measurement of the wave aberrations of the human eye using a Hartmann-Shack wavefront sensor", *Journal of the Optical Society of America, A, 11, pp. 1949-1957*, 1994.
- [22] Malacara, D., *Optical Shop Testing*, Jon Wiley and Sons, Inc, New York.
- [23] Manhan, V., "Zernike Circle Polynomials and Optical Aberrations of Systems with Circular Pupils", *Engineering and Laboratory Notes in Optics and Photonics New*, 1994.
- [24] Perry, S.W., H.S. Wong, and L. Guang, *Adaptive Image Processing: A Computational Intelligence Perspective*, CRC Press, New York, 2002.
- [25] Salmon, T.O., "*Corneal Contribution to the Wavefront Aberration of the Eye*", Doctoral Dissertation, School of Optometry, Indiana University, 1999
- [26] Sonksen, P. M., and A. J. Macrae, "Vision for coloured pictures at different acuities: the Sonksen Picture Guide to Visual Function", *Developmental Medicine Child Neurology*, 29: pp. 337-347, 1987.
- [27] Smirnov, H. S., "Measurement of the Wave Aberration in the Human Eye", *Biophys*, 6: pp. 52-66, 1961.

- [28] Thibos, L. N., “Formation and Sampling of the Retinal Image”, Chapter 1 in *Seeing, A volume in the Handbook of Perception and Cognition Series*, Karen K. De Valois, ed. Academic Press, California, 2000.
- [29] Thibos, L. N., Applegate, R. A., et al. “Standards for Reporting the Optical Aberrations of Eyes”, *Trends in Optics and Photonics, Vol. 35, Vision Science and its Applications*, pp. 110-130, Washington, DC, 2000.
- [30] Tyson, R. K., *Principles of Adaptive Optics*, Academic Press, Boston, 1998.
- [31] Wallman, J., J. I. Adams, and J. Trachtman, “The eyes of young chicks grow towards emmetropia”, *Investigative Ophthalmology and Visual Science*, 20, pp. 557-561, 1981.
- [32] Welford, W.T., *Aberrations of the symmetrical optical system*, Academic Press, London, 1974.
- [33] Williams, C.S., and O.A. Becklund, *Introduction to the Optical Transfer Function*, John Wiley and Sons, New York, 1989.


APPENDICES

Appendix A- Institutional Review Board Approval and Supporting Documents



Division of Sponsored Research & Training
Office of Research Compliance, MARC 430

MEMORANDUM

To: Dr. Armando Barreto & Miguel Alonso Jr.
CC: File
From: Yvette Peterson, Coordinator Institutional Review Board 
Date: January 17, 2003
Proposal Title: Customizable Computer Display for The Visually Impaired
Approval # 011603-00

The Institutional Review Board of Florida International University has approved your study for the use of human subjects. Your annual report will be due January 2004. As a requirement of IRB approval you are required to:

- 1) Provide immediate written notification to the IRB of:
 - Any additions to, or changes in the procedures involving human subjects,
 - Every serious or unusual or unanticipated adverse event as well as problems with the rights or welfare of the human subjects. Confirmation of receipt of serious AE reports must be made with the IRB office.
- 2) Utilize copies of the date stamped consent document(s) for the recruitment of subjects and receive annual renewal of consent documents.
- 3) **Receive annual review and re-approval.**

Special Conditions: None

Please note your approval number is indicated above. For further information, you may contact the IRB Coordinator by email at irbiacuc@fiu.edu or visit the DSRT – Human Subject web site at www.dsrt.fiu.edu.

Figure A-1: IRB Approval

Consent to Participate in a Research Study

Title: Customizable Computer Display for the Visually Impaired

You are being asked to participate in a research project listed above to be conducted at Florida International University with Dr. Armando Barreto as principal investigator. As part of the study, you will be asked to identify various images displayed on the monitor of a computer with, or without glasses, as determined by us. This will take a total of 15 to 20 minutes of your time. You will be participating in this study along with about 50 other students/participants.

The purpose of this research is to develop a technique which will help the visually impaired when using the computer. If you decide to participate in the study, we will tell you what day and time to come to the DSP Lab in the Engineering Center at FIU. The procedure will be as follows: 1) you will be given a 10 minute briefing on the procedure and the purpose of this experiment; 2) you will be seated in front of a digital display, with or without glasses provided by the investigator(s) for no more than 10 minutes, 3) you will be asked to identify several digital images.

The risks involved as a participant in this project are minimal. They are not expected to be beyond the potential (and temporary) discomfort caused by the blurring of your vision during the duration (not to exceed 10 minutes) of the test. Your participation will assist the researcher in gathering knowledge in this area of study. You will not benefit directly from this research. Participation in this study is of no cost to you and you will not be compensated for your time.

You may withdraw your consent and discontinue participation in this research project at any time without any negative consequences. All information pertaining to this study and participation will be kept locked in a password-protected computer. The files generated as part of the study will only be identified by subject number. The results of this research will be presented in group format and no names will be disclosed. Your responses are strictly confidential and would only be disclosed as required by law.

You have the right to ask questions concerning the procedure, and any questions you may have will be answered to the best of our ability. If any new findings are developed during the time that you are in this study which may affect your willingness to continue in the study, you will be informed as soon as possible.

Figure A-2: Consent to participate in a Research Study, part 1



If you desire further information about this research, you should contact Dr. Armando Barreto, Associate Professor in the Department of Electrical and Computer Engineering, at 305-348-3711. If you would like to speak with someone about being a subject in this study, you may contact Dr. Bernard Gertsman, the chairperson of the Institutional Review Board at Florida International University, at 305-348-3115.

Your signature below indicates that all questions have been answered to your liking. You are aware of your rights and you would like to be in the study.

Signature of the Participant	Printed Name	Date
------------------------------	--------------	------

I have explained and defined in detail the research procedure in which the participant has agreed to participate and have offered him a copy of this informed consent form.

Signature of Witness	Date
----------------------	------

Department of Electrical and Computer Engineering
College of Engineering
10555 W. Flagler Street, Miami, FL 33174 • Tel: 305-348-2807 • Fax: 305-348-3707 • www.fiu.edu
Florida International University is an Equal Opportunity/Access Employer and Institution • TDD via FRS 1-800-955-4771

Figure A-3: Consent to participate in a Research Study, part 2

Appendix B- Sample Acuity Scoring Sheet

Acuity Test

Subject Number ██████████

Date ██████████

Standard

Row	Acuity Equivalent		ETDRS Chart R	Eye	
	Snellen	LogMar		O.D.	Right
1	20/200	1	(H) (V) (Z) (D) (S)		
2	20/169	0.9	(N) (C) (V) (K) (D)		
3	20/125	0.8	(C) (Z) (S) (H) (N)		
4	20/100	0.7	(O) (N) (V) (S) (R)		
5	20/80	0.6	(K) (D) (N) (R) (O)		
6	20/63	0.5	(Z) (K) (C) (S) (V)		
7	20/50	0.4	(D) (V) (O) (H) (C)		
8	20/40	0.3	(O) (H) (V) (C) (K)		
9	20/32	0.2	(H) (Z) (C) (K) (O)		
10	20/25	0.1	(N) (X) (K) (H) (X)		
11	20/20	0	(Z) (H) (C) (X) (X)		
12	20/16	-0.1	(X) (X) (X) (X) (X)		
13	20/12.5	-0.2	(X) (X) (X) (X) (X)		
14	20/10	-0.3	(X) (X) (X) (X) (X)		

Figure B-4: Sample Eye Test Scoring Sheet

Appendix C – MATLAB Code

This function, `wnr()`, implements the Minimum Mean Square Error Filter.

```
function J = wnr(varargin)
% USE:
% J = wnr(I,PSf);
% J = wnr(I,PSf,K);
[I, PSF, K] = parse_inputs(varargin{:});

otf = psf2otf(PSF); % psf2otf is a MATLAB function

Denom = abs(otf).^2 + K;
Nomin = conj(otf).*fft(I);

JFT = Nomin./Denom;
J = real(ifft(JFT));

%%%%%%%%%%%%%%%%%%%%%%%%%%%%%%%%%%%%%%%%%%%%%%%%%%%%%%%%%%%%%%%%%%%%%%%%
% Function: parse_inputs
function [I, PSF, K] = ...
    parse_inputs(varargin),
% Outputs: I    the input array (could be any numeric class, 2D, 3D)
%          PSF  operator that applies blurring on the image
%          K    the approximated signal to noise ratio
% Defaults:
K=0;

error(nargchk(2,3,nargin));

% Assign the inputs:
I = varargin{1};%    deconvwnr(A,PSF)
PSF = varargin{2};
switch nargin
case 3,%    deconvwnr(A,PSF,nsr)
    K = varargin{3};
end
```

This function, `p_f()`, implements the generation of the analytical PSF.

```
function [pf,w,otf,psf] = p_f(D,n,WF,x,y,M,pd,wv)
% USE: [pf,w,otf,psf] = p_f(D,n,WF,x,y,M)
% pf is the pupil function
% w is the wavefront aberration function as a matrix of values
% otf is the optical transfer function
% psf is the point spread function
% D is the value of the pupil function, usually a matrix of ones
% n is the index of refraction of the eye
% WF is the symbolic representation of the wavefront aberration in x and y
% x and y are symbolic variables
% M is the magnification factor
% pd is the pupil diameter
% wv is the wavelength of light
```

```

pf=zeros(size(D));
[X,Y]=size(D);
xd=zeros(X,Y);
yd=xd;
pr=pd/2;
for l=1:Y;
    yd(:,l)=linspace(pr*M*1,pr*M*-1,X)';
end
for l=1:X
    xd(l,:)=linspace(pr*M*-1,pr*M*1,Y);
end
w=subs(WF,{x,y},{xd,yd});
if WF == 1
    w=ones(size(D));
end
for l=1:Y
    for k=1:X
        if( sqrt( xd(1,k)^2 + yd(l,1)^2 ) > 1*pr )
            w(k,l)=0;
            D(k,l)=0;
        end
        %D(k,l)=1-sqrt( xd(1,k)^2 + yd(l,1)^2 );
    end
end
pf=D.*exp(-1*j*2*pi*n*w/wv);
for l=1:Y
    for k=1:X
        if( sqrt( xd(1,k)^2 + yd(l,1)^2 ) > 1 )
            pf(k,l)=0;
        end
    end
end
pf1=conj(pf);
otf=ifftn(fft(pf).*fft(pf1));
otf=otf/max(max(otf));
psf=abs(otf2psf(otf));
%psf=ifftn(otf);

```